Title: The influence of heating on the carbon isotope composition, organic geochemistry and petrology of coal from the Upper Silesian Coal Basin (Poland) : an experimental and field study

Author: Justyna Ciesielczuk, Maciej Górka, Monika J. Fabiańska, Magdalena Misz-Kennan, Dominik Jura

Citation style: Ciesielczuk Justyna, Górka Maciej, Fabiańska Monika J., Misz-Kennan Magdalena, Jura Dominik. (2021). The influence of heating on the carbon isotope composition, organic geochemistry and petrology of coal from the Upper Silesian Coal Basin (Poland) : an experimental and field study. “International Journal of Coal Geology” (Vol. 241, 2021, art. no. 103749, s. 1-18), DOI:10.1016/j.coal.2021.103749

International Journal of Coal Geology 241 (2021) 103749

Contents lists available at ScienceDirect

International Journal of Coal Geology

journal homepage: www.elsevier.com/locate/coal

The influence of heating on the carbon isotope composition, organic geochemistry and petrology of coal from the Upper Silesian Coal Basin (Poland): An experimental and field study

Justyna Ciesielczuk [a,*], Maciej Górka [b], Monika J. Fabiańska [a], Magdalena Misz-Kennan [a], Dominik Jura [a]

[a] Faculty of Natural Sciences, University of Silesia in Katowice, Będzińska 60, 41-200 Sosnowiec, Poland
[b] Faculty of Earth Science and Environmental Management, University of Wrocław, Cybulskiego 32, 50-205 Wrocław, Poland

ARTICLE INFO

Keywords:
Coal and coal-bearing rocks
Heating conditions generated naturally and experimentally
$\delta^{13}C$ signature
Organic geochemistry
Upper Silesian Coal Basin
Poland

ABSTRACT

The impact of natural intra-deposit heating on the $\delta^{13}C$ signature, organic geochemistry, and petrology of coal and coal-bearing rocks characterised by various degrees of coalification and palaeoenvironments in the Upper Silesian Coal Basin, Poland, is elaborated. Reconstruction of palaeofire performed by heating experiments up to 400 °C in open and semi-closed systems with different heating regimes confirms the crucial significance of temperature and oxygen access. In open-system heating, released ^{13}C-depleted gases enrich residue coke in ^{13}C compared to raw coal. Petrological examinations did not show the impact of palaeofires on the maceral properties of coal. However, the carried-out experiment caused the formation of devolatilisation pores, rounded edges, cracks, pale rims, as well as higher reflectance and paler colour that was what was expected. Extractable compounds become highly depleted, and low-weight organic compounds nearly absent. Relatively high contents of combustion-formed PAHs are an indicator of open-system heating. In semi-closed systems, the final total isotopic composition was almost unchanged as no components are carried away though changes in petrography and geochemistry occur. Increased extract yields reflect the release of bitumen from closed pores and partial pyrolysis of organic matter. Depletion of lighter *n*-alkane compounds, total carbon TC and volatiles decrease, and variable values of various alkyl aromatic hydrocarbon ratios are also indicative of semi-closed heating. Coal seams suspected of intra-deposit heating show geochemical and isotopic features similar to semi-closed- rather than open-system heating, and their $\delta^{13}C$ signatures and organic geochemistry did not respond strongly during laboratory re-heating.

1. Introduction

The Upper Silesian Coal Basin (USCB) in Poland and the Czech Republic was formed in paralic and limnic environments in Late Carboniferous at the north-eastern periphery of the Variscan Mountain Belt. The thickness of the Namurian and Westphalian coal-bearing deposits ranges from less than 1 km in the eastern part up to ca 8.5 km in the western part with 4.7 km in the centre Figs 1 and 2. In the southern part of the basin, weathered and eroded deposits were covered by sediments of Miocene Carpathian Foredeep (Jura, 2001; Jureczka et al., 2005).

Coals in the USCB vary, inter alia, in rank, maceral- and mineral composition, and their propensity for self-heating. In general, coalification increases vertically with depth and laterally towards the western part of the basin. Average values of vitrinite reflectance R_r increase with depth from 0.56–2.00% at 0.2%/km. The coals are representative of all coal-bearing sequences of Carboniferous age in USCB, i.e., the latest Mississippian mudstone paralic series and Pennsylvanian limnic sandstone- and mudstone series. The dominant maceral group is vitrinite accompanied by everpresent liptinite; however, the contents of inertinite macerals can reach 55% in some beds (Jurczak-Drabek, 1996; Gabzdyl et al., 1997).

In the south-western USCB, some coal seams of the Upper Silesian Sandstone Series exhibit reduced thicknesses or thin out (Figs. 1 and 2). Altered breccias, varied in colour, occur above these thinning coal

* Corresponding author.
E-mail addresses: justyna.ciesielczuk@us.edu.pl (J. Ciesielczuk), maciej.gorka@uwr.edu.pl (M. Górka), monika.fabianska@us.edu.pl (M.J. Fabiańska), magdalena.misz@us.edu.pl (M. Misz-Kennan), dominik.jura@us.edu.pl (D. Jura).

https://doi.org/10.1016/j.coal.2021.103749
Received 4 December 2020; Received in revised form 14 April 2021; Accepted 15 April 2021
Available online 19 April 2021

seams, and any coal present is grey-black, dull, heavily cracked, brittle, and without a banded structure (Fig. 2c). Thermally transformed coal-bearing rocks are typically characterised by increased fracturing, porosity, and changes in physical-, chemical- and mechanical properties, and in petrological- and geochemical parameters or indicators. These features suggest that some USCB coals were heated after deposition (Gabzdyl and Probierz, 1987; Klika and Kraussová, 1993; Klika et al., 2004; Martinec et al., 2005; Muszyński et al., 2006). The cause of heating affecting coals beyond the geothermal gradient can be igneous intrusions or interaction with hydrothermal systems (e.g., Rahman et al., 2018; Sanders and Rimmer, 2020; Valentim et al., 2020; Yoksoulian et al., 2016). Based on organic geochemistry, petrography, palaeomagnetism, and Ar—Ar data performed on samples deriving from the USCB, the most probable reason was palaeofire (Ciesielczuk et al., 2017, 2020).

Investigations of natural underground fires in coal seams have focused mainly on the geochemical parameters of burning gases (Engle et al., 2012), the composition of gases in terms of carbon isotopes (Brasseur et al., 2002), or the geological history of natural fires (Heffern and Coates, 2004) rather than on the coal residuum. However, the changes in thermal maturity of organic matter assessed by means of organic geochemistry may better define the impact of temperature increase in a deposit caused by phenomena other than the geothermal gradient. For example, aliphatic- and aromatic biomarkers seem to be sensitive to local thermal abnormalities (Arora et al., 2017; Patra et al., 2018). Also, rapid thermal stress can affect the entire composition of sedimentary organic matter since it leads to hydrothermal-bitumen expulsion (Simoneit, 1993).

To reflect conditions of the possible intra-deposit fire caused by self-heating of coals at the given coalification stage, the heating experiment has been carried out with or almost without oxygen access. Since the process requires oxygen access initially, the heating was carried out in the open system. However, in the later stages, oxygen will be exhausted, so the semi-closed system was used to simulate such conditions. The selected temperatures correspond to those that induce devolitization. Varying temperature regimes reflect different heat impacts within a deposit – severe in the case of the open fire and more gentle in the case of low-oxygen conditions.

The main aim of our work was to show the influence of heating under various conditions on the C isotope composition, organic geochemistry generally, and the organic- and mineral matter of coal-bearing samples representative of various stratigraphic sequences, degrees of coalification, and palaeoenvironments. A secondary goal was to compare the experimental data with the characteristics of rocks from an area affected by a rapid local increase in temperature in the geological past (as opposed to the regional geothermal gradient). We hypothesised that thermally-altered coal preserves the influence of heating in its $\delta^{13}C$ signature as well as in its organic-matter characteristics. Specifically, the aim was to identify any compositional trends by reference to heating experiments both in open and semi-closed environments.

2. Materials and methods

Fifteen samples of raw bituminous coals (11 samples) and coal-bearing rocks (4 samples with sample symbols marked with ˆ) were collected. Twelve of these came from five underground coal mines operating in the south-western (Jankowice mine (J3, J4), Marcel (M3, Mˆ7, M9, M11, and M12)) and the north-eastern part of the USCB

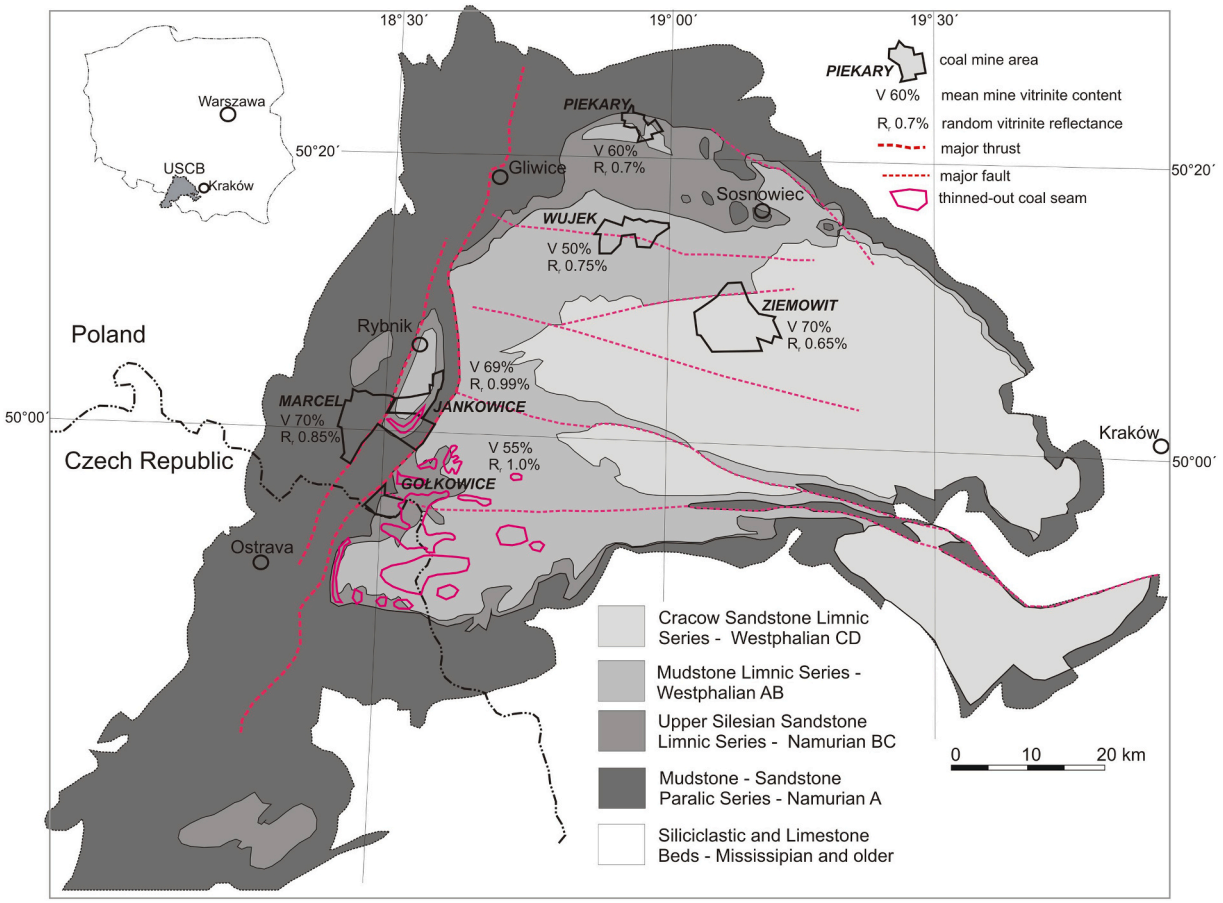

Fig. 1. A sketch of the Upper Silesian Coal Basin geological formations with coal-mine locations and mean mine vitrinite content and random vitrinite reflectance (modified after Jura, 2001; Jurczak-Drabek, 1996; Jureczka et al., 2005).

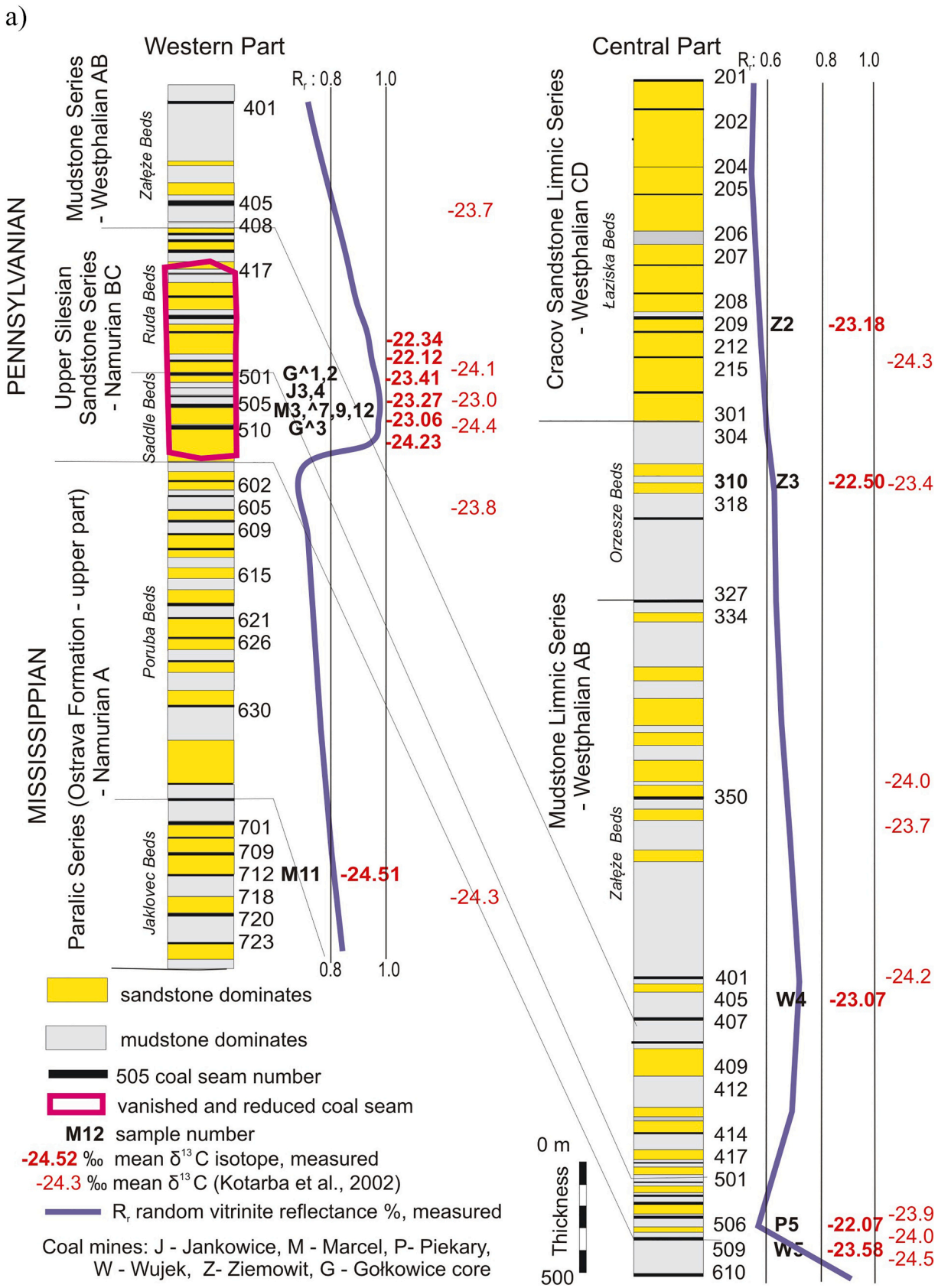

Fig. 2. Samples locations in A - generalised columnar section of the Carboniferous formations in the Upper Silesian Coal Basin and B – NNW-SSE schematic cross-section of the Jankowice and Marcel Coal Mines, according to the mine geological documentation (2001). Thinned-out parts of coal seams are marked in purple. C – Breccias above thinned coal seam 505, Marcel Coal Mine. (For interpretation of the references to colour in this figure legend, the reader is referred to the web version of this article.)

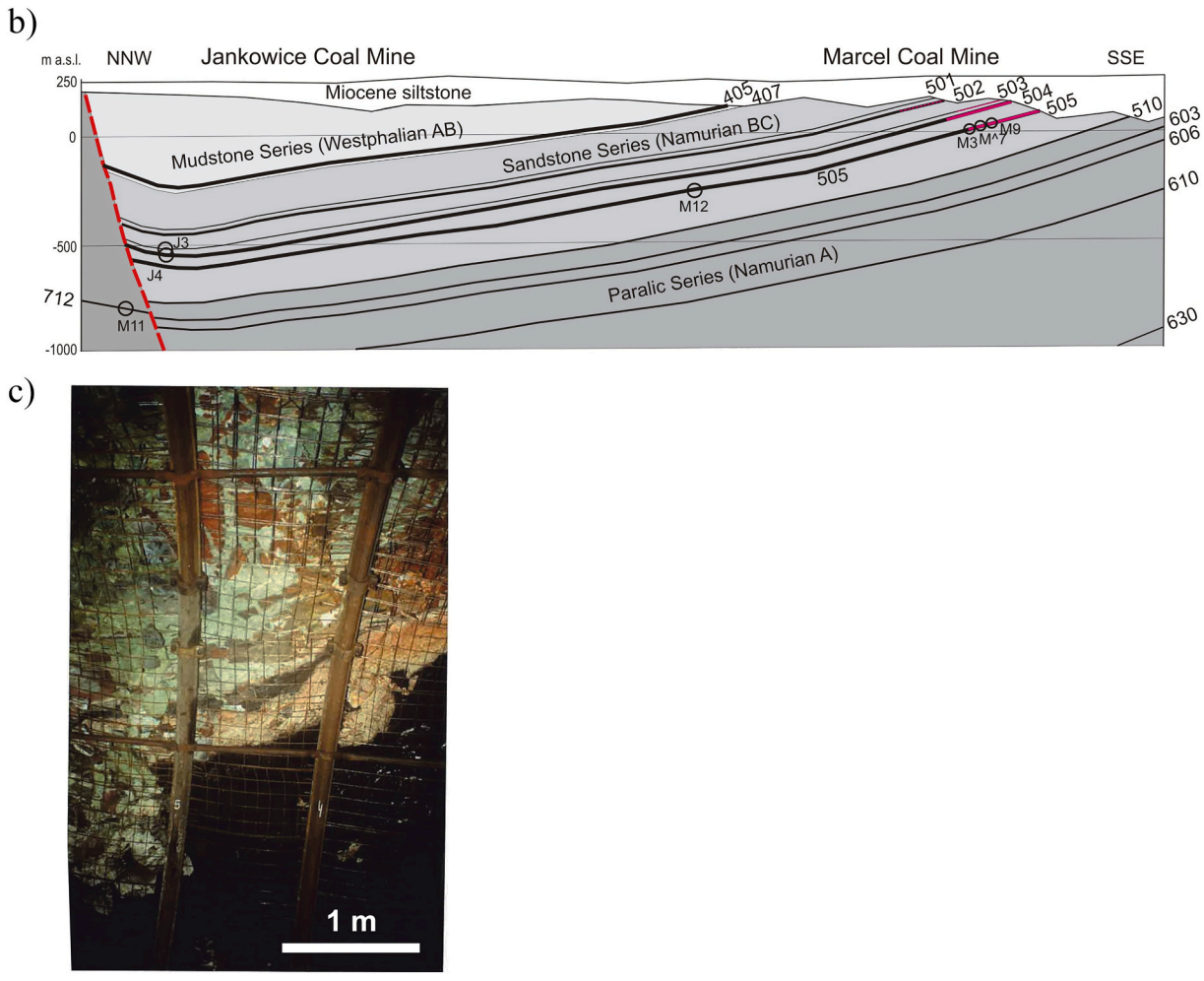

Fig. 2. (*continued*).

(Ziemowit (Z2, Z3), Wujek (W4, W5), and Piekary (P5)). The other three (Gˆ1, Gˆ2, and Gˆ3) came from the Gołkowice IV core drilled next to the thermally reduced 501–505 seams. The samples represent coal seams ranging from the oldest 712 (M11), through 505 (M12) to 504 and 503 (J4 and J3, respectively) in the SW part and 509 (W5), 506 (P5), 404/5 (W4), 309 (Z3) to the youngest 209 (Z2) in NE part. The actual sampling depth ranges from ca 1000 m subsurface (M11) to ca 250 m subsurface (Table 1; Figs. 1, 2).

The coals differ in lithotype (clarain, vitrain and durain), vitrinite reflectance R_r (0.56–0.99%), petrographic- and chemical composition and potential influence of thermal heating (Tables 1, 2, and 3). Three samples are collected from part of the coal seam 505, which is thermally-affected (samples M3, Mˆ7 and M9), and one (sample Gˆ3) macroscopically shows changes in colour. Other samples showed no signs of macroscopic change. However, for some samples with the macroscopically unchanged appearance (M12, J3, J4, W5, P5, Gˆ1, and Gˆ2) located in the same coal seam at varying distances (horizontal and vertical) from a thinned-out part, the investigated parameters, sensitive to the slightest thermal influence, were expected to prove the full extent of the thermal aureole.

The heating experiment has been carried out with or almost without oxygen access. All samples were heated in an open system for 24 h and in a semi-closed system for 2 h. About 2.0 g of a powdered sample of grain size <0.2 mm was used in all cases. For the open system heating, the sample was placed in an open crucible, put into a preheated oven and heated at 400 °C in a chamber muffled furnace (FCF 2,55SHM, prod. Czylok) for 24 h. The semi-closed system procedure involved heating the sample placed in the semi-closed steel retort in a tubular muffled furnace. The retort allowed gases to escape but limited oxygen access to the heated sample. The heating rate in the semi-closed system was 20 °C/min up to 400 °C. When the final temperature was reached, the isothermal heating followed for two hours. In the open system, the samples were placed in an oven pre-heated to 400 °C and heated isothermally at this temperature.

Petrographic- and geochemical properties and isotope compositions were determined for both raw- and heated samples. Mineral and chemical compositions were determined for eight raw samples, all coal-bearing rocks and the selected four coals, among which two had been heated naturally.

For petrography, polished blocks were prepared according to procedures described in ISO 7404-2 (2009). Raw coal samples were crushed to <1 mm and embedded in epoxy resin. After hardening, they were ground using grinding paper of decreasing size 53.5 μm, 23.6 μm, and 16 μm that was followed by polishing using diamond paste. Samples surface quality was examined using a dry objective microscope prior to microscopic examination. Material obtained from the heating experiments was also embedded in epoxy resin and polished blocks prepared according to the same procedure.

The prepared samples were examined, using reflected white light and fluorescence, with a Zeiss Axioplan2 microscope at 500× magnification. The content of maceral groups and mineral matter was determined at 500 points evenly distributed over the sample surface following the procedures described in ISO 7404-3 (2009). Samples obtained from the heating experiments contained altered organic matter

Table 1
Raw-sample characteristics and results of heating experiments in open (o) and semi-closed (c) systems on bituminous coal- and coal-shale samples from the Upper Silesian Coal Basin.

No sample	Seam	Depth m subsurface	Lithotype	$\delta^{13}C$ ‰	TC[a] %	TS[a] %	TOC[daf] %	Extract/pyrolysate yield %wt.	Volatile matter[a] %
J3	503	ca 800	clarain	−23.41	57.60	0.40	74.04	0.34	22.14
J3o				−22.05	40.40	0.40		0.02	
J3c				−23.24	82.80	0.50		0.52	
J4	504	ca 820	vitrain	−23.27	82.30	0.40	82.96	0.28	26.45
J4o				−21.98	66.20	0.40		0.05	
J4c				−22.89	54.40	0.30		0.71	
M3	505	ca 250	durain	−23.64	63.40	1.00	63.91	0.57	37.84
M3o				−23.29	59.90	1.80		0.05	
M3c				−23.48	73.80	1.20		0.09	
M^7	505	ca 250	coal shale	−23.05	8.10	0.80	50.63	0.07	12.80
M^7o				−21.42	3.90	0.30		0.01	
M^7c				−26.14	18.90	1.90		0.01	
M9	505	ca 250	durain	−23.52	66.30	0.10	67.11	0.55	37.81
M9o				−23.20	61.80	1.40		0.01	
M9c				−23.52	75.00	0.60		0.03	
M11	712	ca 1000	vitrain	−24.51	82.50	0.40	85.23	2.51	35.07
M11o				−15.52	3.70	1.70		0.02	
M11c				−24.54	84.50	0.40		0.15	
M12	505	ca 500	clarain	−23.06	84.60	0.20	85.28	0.94	25.27
M12o				−22.49	74.80	0.00		0.02	
M12c				−23.13	36.00	0.60		0.34	
Z2	209	ca 500	clarain	−23.18	69.40	0.90	88.30	3.51	37.01
Z2o				−14.77	2.80	5.30		0.06	
Z2c				−22.86	80.50	0.60		0.80	
Z3	309	ca 550	clarain	−22.50	70.80	0.10	71.66	3.03	39.79
Z3o				−12.71	4.80	2.20		0.05	
Z3c				−22.67	77.30	1.00		0.74	
W4	404/5	ca 670	clarain	−23.03	77.40	0.60	81.30	2.91	35.20
W4o				−22.29	57.20	0.50		0.07	
W4c				−23.11	74.90	0.70		0.52	
W5	509	ca 700	vitrain	−23.58	82.60	0.50	82.60	4.57	34.43
W5o				−22.61	8.60	2.40		0.25	
W5c				−23.13	67.40	7.80		0.67	
P5	506	ca 600	clarain	−22.07	68.80	2.90	74.46	6.84	36.76
P5o				−20.14	3.10	2.60		0.07	
P5c				−22.32	68.30	5.30		0.52	
G^1	501	ca 770	durain	−22.34	55.40	0.80	56.19	0.80	12.20
G^1o				−22.51	1.00	0.10		0.02	
G^1c				−22.35	53.10	0.60		0.12	
G^2	502	ca 780	coal shale	−22.12	26.30	0.30	109.58	1.35	15.01
G^2o				−19.23	0.60	0.30		0.03	
G^2c				−22.05	24.50	0.30		0.11	
G^3		ca 890	clarain	−24.23	39.10	1.00	47.22	0.67	16.52
G^3o				−14.46	0.30	0.20		0.01	
G^3c				−24.24	35.70	0.60		0.08	

a – analytical basis, daf – dry ash free, recalculated for organic matter.

and minerals. Their content was established at 500 points in each sample. To determine the rank of organic matter, vitrinite reflectance measurements (R_r) were taken at 100 points in each sample following the methodology described in ISO 7404-5 (2009). Reflectance measurements were also taken at 50–100 points to determine the degree of alteration of organic matter; some samples contained none (Table 2). All petrographic analyses were carried out in the Institute of Earth Sciences at the University of Silesia, Poland.

For geochemistry, both raw- and heated rocks and coals were powdered to <0.20 mm and extracted with dichloromethane (DCM; Avantor, analytical grade) in an ultrasonic bath (3–4 times of 15 min each). Extracts from subsequent extractions of each sample were pooled together, dried out at an ambient temperature and weighed. Extraction yields are given in Table 1.

An Agilent 6890 gas chromatograph with an HP-5 column (60 m × 0.25 mm i.d.), coated with a 0.25-μm stationary phase film coupled with an Agilent 5973 mass spectrometer, was used. The experimental conditions were as follows: carrier gas, He; temperature, 50 °C (isothermal for 2 min); heating rate to 175 °C at 10 °C/min, to 225 °C at 6 °C/min and, finally, to 300 °C at 4 °C/min. The final temperature (300 °C) was maintained for 20 min. The mass spectrometer was operated in electron impact ionisation mode at 70 eV and scanned from 50 to 650 da. Data were acquired in full scan mode and processed with Hewlett Packard Chemstation software. The compounds were identified using their mass spectra, comparing peak retention times with those of standard compounds, interpretation of MS fragmentation patterns, and data from the literature (Philp, 1985; MDS Data, 2012). Geochemical parameters were calculated using peak areas acquired in the manual integration mode. All geochemical analyses were carried out in the Institute of Earth Sciences at the University of Silesia, Poland.

A combustion module (CM) coupled with a cavity ring-down spectroscopy (CRDS) system (G2201-i analyser, Picarro Inc.) was used for the carbon-isotope analysis carried out in the Institute of Geological Sciences at the University of Wrocław. After burning the sample in tin capsules at 980 °C, purified CO_2 was collected using an interface (carrier gas - N_2) and sent to the isotopic analyser. Liu et al. (2018) confirmed the relationship between the C concentration and the final $\delta^{13}C$ value. Due to variable C content, a sample amount in each run was tested experimentally to obtain ca 2000–4000 ppm of CO_2 signal. All $\delta^{13}C$ values were reported following multi-point normalisation (Coplen et al., 2006; Skrzypek, 2013) to the VPDB scale based on international standards NBS-19, NBS-18, IAEA CO-8, USGS-24, USGS-40, and LSVEC. For a

Table 2
Petrographic composition of bituminous coal and coal-bearing samples heated in open (o) and semi-closed (c) systems.

Sample No.	Vitrinite (%)	Liptinite (%)	Inertinite (%)	Natural chars (%)	Paler in colour vitrinite (%)	Plasticised particles (%)	Inertinite in paler in colour particles (%)	Brighter oxidation rims around the edge of the particle (%)	Particles with pores (%)	Particles with pores and brighter oxidation rims (%)	Particles with cracks (%)	Particles with cracks and brighter oxidation rims (%)	Strongly altered organic matter (%)	Sum of organic matter[1] (%)	Mineral matter (%)	R_r (%)	SD
J3	69.0	4.8	2.6	1.4	0.0	0.0	0.0	0.0	0.0	0.0	0.0	0.0	0.0	77.8	22.2	0.99	0.04
J3o	0.0	0.0	5.4	0.0	24.2	0.0	0.8	0.0	28.6	0.0	0.0	0.0	10.8	69.8	30.2	1.80	0.15
J3c	5.2	1.8	4.6	0.0	27.2	0.0	1.8	0.0	0.0	0.0	0.0	0.0	59.0	99.6	0.4	1.67	0.73
J4	70.6	4.8	23.6	0.0	0.0	0.0	0.0	0.0	0.0	0.0	0.0	0.0	0.0	99.2	0.8	0.91	0.04
J4o	0.0	0.0	0.0	0.0	19.8	0.0	0.0	0.0	62.2	0.0	11.8	0.0	0.0	99.8	0.2	1.74	0.19
J4c	27.4	1.4	8.6	0.0	14.8	4.2	0.0	0.0	15.4	0.0	0.0	0.0	4.0	75.8	24.2	1.23	0.28
M3	48.8	9.6	40.8	0.0	0.0	0.0	0.0	0.0	0.0	0.0	0.0	0.0	0.0	99.2	0.8	0.85	0.06
M3o	0.0	0.0	0.0	0.0	36.0	0.0	0.0	0.0	0.0	0.0	0.0	41.0	0.0	77.0	23.0	1.25	0.15
M3c	6.0	1.2	5.8	0.0	38.6	0.0	5.6	0.0	0.0	0.0	0.0	0.0	42.4	99.6	0.4	1.52	0.43
Mˆ7	4.2	8.2	3.6	0.0	0.0	0.0	0.0	0.0	0.0	0.0	0.0	0.0	0.0	16.0	84.0	0.91	0.04
Mˆ7o	0.0	0.0	0.0	0.0	0.0	0.0	0.0	0.0	0.0	0.0	0.0	0.0	0.0	0.0	100.0	–	–
Mˆ7c	0.0	0.0	0.0	0.0	23.8	0.0	0.0	0.0	0.0	0.0	0.0	0.0	0.0	23.8	76.2	1.90	0.21
M9	38.0	8.6	52.2	0.0	0.0	0.0	0.0	0.0	0.0	0.0	0.0	0.0	0.0	98.8	1.2	0.87	0.07
M9o	0.0	0.0	0.0	0.0	77.6	0.0	2.4	0.0	0.0	0.0	0.0	0.0	0.0	80.0	20.0	1.26	0.12
M9c	0.0	3.0	27.8	0.0	45.0	0.0	19.6	0.0	1.4	0.0	2.4	0.0	0.0	99.2	0.8	1.58	0.23
M11	72.6	12.6	11.6	0.0	0.0	0.0	0.0	0.0	0.0	0.0	0.0	0.0	0.0	96.8	3.2	0.80	0.03
M11o	0.0	0.0	0.0	0.0	0.0	0.0	0.0	0.0	0.0	0.0	0.0	0.0	2.0	2.0	98.0	1.91	0.38
M11c	0.0	0.0	0.0	0.0	29.8	22.8	5.0	0.0	42.2	0.0	0.0	0.0	0.0	99.8	0.2	1.65	0.30
M12	24.4	7.8	67.0	0.0	0.0	0.0	0.0	0.0	0.0	0.0	0.0	0.0	0.0	99.2	0.8	0.82	0.04
M12o	0.0	0.0	0.0	0.0	34.6	0.0	11.4	10.8	18.2	4.0	2.2	5.0	0.0	86.2	13.8	2.02	0.25
M12c	20.0	4.0	14.0	0.0	14.4	0.0	6.4	0.0	41.0	0.0	0.0	0.0	0.0	99.8	0.2	2.02	0.71
Z2	56.4	6.6	15.6	0.0	0.0	0.0	0.0	0.0	0.0	0.0	0.0	0.0	0.0	78.6	21.4	0.56	0.04
Z2o	0.0	0.0	0.0	0.0	0.0	0.0	0.0	0.0	0.0	0.0	0.0	0.0	0.0	0.0	100.0	–	–
Z2c	6.2	0.0	1.8	0.0	44.6	0.0	13.4	0.0	32.8	0.0	0.0	0.0	0.0	98.8	1.2	1.79	0.35
Z3	68.2	7.6	23.0	0.0	0.0	0.0	0.0	0.0	0.0	0.0	0.0	0.0	0.0	98.8	1.2	0.61	0.03
Z3o	0.0	0.0	0.0	0.0	0.0	0.0	0.0	0.0	0.0	0.0	0.0	0.0	0.0	0.0	100.0	–	–
Z3c	11.2	1.0	3.0	0.0	41.8	0.4	6.6	0.0	32.0	0.0	0.2	0.0	0.0	96.2	3.8	1.74	0.46
W4	73.4	8.0	13.8	0.0	0.0	0.0	0.0	0.0	0.0	0.0	0.0	0.0	0.0	95.2	4.8	0.72	0.03
W4o	0.0	0.0	0.0	0.0	62.8	0.0	7.4	11.0	11.4	1.8	0.2	2.0	0.0	96.6	3.4	1.97	0.18
W4c	0.8	0.0	0.8	0.0	49.0	0.0	9.8	0.0	35.8	0.0	0.0	0.0	0.0	96.2	3.8	1.65	0.22
W5	79.4	3.6	17.0	0.0	0.0	0.0	0.0	0.0	0.0	0.0	0.0	0.0	0.0	100.0	0.0	0.85	0.03
W5o	0.0	0.0	1.2	0.0	0.0	0.0	0.0	0.0	0.0	0.0	0.0	0.0	0.0	1.2	98.8	–	–
W5c	1.8	0.2	0.6	0.0	40.8	2.2	8.2	0.0	44.4	0.0	0.0	0.0	0.0	98.2	1.8	2.12	0.30
P5	74.2	10.6	7.6	0.0	0.0	0.0	0.0	0.0	0.0	0.0	0.0	0.0	0.0	92.4	7.6	0.58	0.04
P5o	0.4	0.0	1.2	0.0	2.4	0.0	0.0	0.0	0.0	0.0	0.0	0.0	0.0	4.0	96.0	2.49	0.60
P5c	16.4	2.8	8.8	0.0	46.8	0.0	2.4	0.0	16.6	0.0	3.8	0.0	0.0	97.6	2.4	1.63	0.54
Gˆ1	33.4	10.2	55.0	0.0	0.0	0.0	0.0	0.0	0.0	0.0	0.0	0.0	0.0	98.6	1.4	0.92	0.05
Gˆ1o	0.0	0.0	0.0	0.0	0.0	0.0	0.0	0.0	0.0	0.0	0.0	0.0	1.0	1.0	99.0	1.56	0.32
Gˆ1c	19.8	0.6	2.2	0.0	11.2	9.6	5.8	0.0	31.4	0.0	0.0	0.0	0.0	80.6	19.4	1.65	0.65
Gˆ2	10.8	1.8	11.4	0.0	0.0	0.0	0.0	0.0	0.0	0.0	0.0	0.0	0.0	4.0	76.0	0.99	0.04
Gˆ2o	0.0	0.0	0.2	0.0	0.0	0.0	0.0	0.0	0.0	0.0	0.0	0.0	0.4	0.6	99.4	1.73	0.29
Gˆ2c	0.0	0.0	0.0	0.0	20.4	0.0	13.0	0.0	9.0	0.0	0.0	0.0	0.0	42.4	57.6	1.86	0.24
Gˆ3	81.8	0.4	0.6	0.0	0.0	0.0	0.0	0.0	0.0	0.0	0.0	0.0	0.0	82.8	17.2	0.97	0.03
Gˆ3o	0.0	0.0	0.0	0.0	0.0	0.0	0.0	0.0	0.0	0.0	0.0	0.0	0.0	0.0	100.0	–	–
Gˆ3c	0.0	0.0	0.0	0.0	20.8	1.4	0.0	0.0	31.0	0.0	0.0	0.0	0.0	53.4	46.6	1.45	0.23

- reflectance was not measured due to absence of organic matter.
[1] sum of values from columns 2–14.

Table 3
Chemical composition of raw samples of coal (J3, J4, M3, M9) and coal-bearing rocks (Mˆ7, Gˆ1, Gˆ2, Gˆ3). Higher values are marked in bold and explained.

Analyte	Unit	J3	J4	M3	M9	Mˆ7	Gˆ1	Gˆ2	Gˆ3	Possible cause or mode of occurrence
SiO_2	%	11.01	1.86	1.16	0.74	**47.08**	**35.99**	**38.42**	**37.01**	quartz, kaolinite, muscovite
TiO_2	%	0.25	0.06	0.03	<0.01	**0.88**	**0.68**	**0.75**	**0.66**	anatase
Al_2O_3	%	5.20	1.42	0.97	0.63	**23.54**	**16.95**	**20.04**	**18.92**	feldspars, muscovite, kaolinite
Fe_2O_3	%	0.66	0.84	**1.09**	**1.14**	**2.26**	**1.24**	**1.98**	**2.39**	pyrite, hematite, siderite
MnO	%	<0.01	0.02	<0.01	<0.01	<0.01	<0.01	0.02	0.01	
MgO	%	0.30	0.70	0.50	0.50	0.44	0.43	0.69	0.70	chlorite, Mg-siderite
CaO	%	0.25	**1.45**	**1.83**	**1.93**	0.11	0.09	0.08	0.17	gypsum
Na_2O	%	0.15	0.14	**0.92**	**0.81**	0.30	0.28	0.19	0.18	natroalunite
K_2O	%	0.64	0.04	0.03	<0.01	**2.44**	**1.83**	**2.26**	**4.92**	muscovite
P_2O_5	%	0.02	<0.01	0.03	<0.01	0.06	0.05	0.07	0.06	apatite
Cr_2O_3	%	0.005	<0.002	<0.002	<0.002	**0.021**	**0.014**	**0.016**	**0.015**	affinity to chlorite
LOI	%	81.4	92.8	91.7	92.0	22.7	42.3	35.3	34.7	coal
Sum	%	99.94	99.36	98.49	98.06	99.85	99.86	99.87	99.85	
Be	PPM	1	<1	<1	<1	**4**	**5**	**4**	**10**	
Sc	PPM	5	2	<1	<1	**19**	**20**	**18**	**18**	
V	PPM	58	32	18	40	**174**	**178**	**145**	**160**	affinity to K-bearing minerals
Co	PPM	13.5	10.7	2.3	**55.3**	**33.4**	**6.8**	**10.1**	**29.0**	affinity to Fe oxides
Ni	PPM	7.5	5.6	**10.4**	**79.7**	**43.0**	**15.9**	**26.7**	**56.9**	pyrite
Cu	PPM	**30.2**	**14.3**	7.2	4.5	**78.7**	**117.6**	**69.3**	**79.2**	chalcopyrite
Zn	PPM	17	9	7	**172**	**59**	26	**85**	**113**	sphalerite
Ga	PPM	6.7	2.9	1.5	<0.5	**25.5**	**21.5**	**23.8**	**23.6**	
As	PPM	<0.5	<0.5	<0.5	<0.5	**5.6**	**8.3**	**3.6**	**35.5**	affinity to hematite
Se	PPM	0.9	0.8	**8.9**	**37.5**	**9.8**	0.7	<0.5	0.7	
Rb	PPM	39.7	1.9	2.8	1.3	**127.8**	**132.2**	**121.9**	**187.9**	affinity to K-bearing minerals
Sr	PPM	56.5	74.1	**547.5**	**565.0**	**138.7**	**121.0**	**147.3**	**105.9**	barite, feldspars
Y	PPM	8.2	6.6	2.4	1.5	**40.1**	**32.6**	**29.6**	**35.5**	
Zr	PPM	32.9	6.0	27.7	2.6	**147.5**	**111.8**	**104.9**	**97.2**	zircon
Nb	PPM	4.0	1.3	2.6	<0.1	**13.3**	**9.9**	**9.8**	**14.9**	
Mo	PPM	1.0	0.9	**3.4**	**5.4**	0.7	0.8	0.4	0.6	
Ag	PPM	0.1	<0.1	<0.1	0.2	0.2	0.3	<0.1	0.2	
Cd	PPM	0.1	<0.1	<0.1	0.5	0.3	<0.1	0.6	0.3	
Sn	PPM	1	<1	<1	<1	**5**	**3**	**4**	**4**	affinity to Fe oxides
Sb	PPM	0.3	0.1	<0.1	<0.1	0.3	**1.3**	0.5	**1.9**	
Cs	PPM	7.5	0.1	0.4	0.1	**16.6**	**27.8**	**17.5**	**16.8**	
Ba	PPM	140	105	**2386**	**2697**	**471**	**340**	**348**	**616**	barite, feldspars
La	PPM	**13.3**	**5.2**	3.1	3.0	**53.1**	**42.3**	**39.7**	**35.2**	
Ce	PPM	**25.8**	**11.4**	5.0	2.1	**102.9**	**78.2**	**79.5**	**74.4**	
Pr	PPM	**2.71**	**1.29**	0.63	0.22	**12.01**	**9.29**	**9.06**	**8.54**	
Nd	PPM	**9.8**	**5.2**	2.3	0.8	**45.8**	**34.2**	**33.6**	**33.4**	
Sm	PPM	**2.02**	**1.07**	0.35	0.11	**8.95**	**6.41**	**6.97**	**6.65**	
Eu	PPM	**0.42**	**0.29**	0.09	<0.02	**1.91**	**1.54**	**1.54**	**1.50**	
Gd	PPM	**1.70**	**1.23**	0.45	0.23	**8.03**	**5.69**	**6.68**	**6.20**	
Tb	PPM	**0.27**	**0.20**	0.07	0.03	**1.37**	**0.96**	**0.99**	**1.00**	
Dy	PPM	**1.47**	**1.23**	0.31	0.15	**7.41**	**6.11**	**5.72**	**6.34**	
Ho	PPM	**0.29**	**0.22**	0.09	0.03	**1.59**	**1.29**	**1.13**	**1.38**	
Er	PPM	**0.94**	**0.69**	0.24	0.06	**4.48**	**3.45**	**3.36**	**4.30**	
Tm	PPM	**0.14**	**0.09**	0.04	0.01	**0.69**	**0.50**	**0.48**	**0.60**	
Yb	PPM	**0.91**	**0.53**	0.23	0.07	**4.39**	**3.38**	**3.14**	**4.33**	
Lu	PPM	0.14	0.08	0.04	0.01	**0.62**	**0.48**	**0.49**	**0.64**	
Hf	PPM	0.8	0.1	0.8	0.1	**4.1**	**3.0**	**3.2**	**2.8**	
Ta	PPM	0.3	<0.1	0.3	0.1	**1.0**	**0.8**	**1.1**	**0.9**	
W	PPM	0.9	0.6	0.5	<0.5	**2.5**	**2.5**	**2.3**	**4.3**	
Au	PPB	<0.5	<0.5	**0.8**	<0.5	<0.5	**1.1**	<0.5	<0.5	
Hg	PPM	0.03	0.01	**0.16**	0.05	**0.12**	**0.08**	**0.17**	**0.14**	
Tl	PPM	<0.1	<0.1	0.2	0.7	0.4	<0.1	<0.1	0.2	
Pb	PPM	**71.0**	**13.0**	9.4	3.5	**38.8**	**53.6**	**28.0**	**41.1**	elemental Pb
Bi	PPM	0.5	0.2	0.2	<0.1	0.8	1.1	0.6	0.9	
Th	PPM	4.7	1.7	4.0	0.2	**15.3**	**15.7**	**16.3**	**14.9**	
U	PPM	2.4	1.1	1.2	<0.1	**7.5**	**7.6**	**5.1**	**6.4**	

greater spread and more precisely normalised $\delta^{13}C$ values, an internal laboratory standard was prepared based on a 6-point international standard calibration curve. The $\delta^{13}C$ values of five new additionally calibrated laboratory standards (chosen from those most enriched in ^{13}C) were: xylitol, − 9.69 ± 0.04‰; cane sugar, −11.13 ± 0.05‰; atropine, 18.80 ± 0.04‰; beet sugar, − 26.03 ± 0.05‰; and caffeine, − 35.16 ± 0.08‰. Therefore, for super-precise testing of the CM-CRDS measurements and final normalisation, a maximum 11-point calibration curve was used. Analytical uncertainty was <0.1‰ for $\delta^{13}C$.

Total carbon (TC), total inorganic carbon (TIC) and total sulphur (TS) were determined using an Eltra CS-500 IR analyser with a TIC module in the Institute of Earth Sciences at the University of Silesia, Poland. TC and TIC were determined using an infrared cell detector for CO_2 and TS for SO_2. Determination of TC and TS was based on the combustion of organic matter in an oxygen atmosphere with simultaneous thermal decomposition of minerals. Determination of TIC was carried out via the reaction of carbonates with 15% warm hydrochloric acid and was equal to 0. The instrument was calibrated in accordance with Eltra standards. Total organic carbon (TOC) was recalculated for organic matter (Table 1).

Chemical composition was performed for raw samples of all coal-bearing rocks and four selected coals. Samples were crushed, averaged

and powdered according to the standard laboratory rules by AcmeLabs. Whole-rock major elements and loss on ignition were measured by ICP-ES and trace elements by ICP-ES/MS by AcmeLabs, Canada. (Table 3).

Mineral phases were identified by powder X-ray diffraction (XRD) and scanning electron microscopy (SEM) (Table 3). Phase compositions of powdered samples were determined using a fully automated Philips PW 3710 X-ray diffractometer operated at 45 kV and 30 mA, with CuKα radiation, and equipped with a graphite monochromator. X'Pert High-Score Plus software with the PDF-4+ database was used to identify and quantify mineral phases. The composition of minerals dispersed within coal was examined using a Philips XL30 ESEM/TMP scanning electron microscope coupled with an energy-dispersive spectrometer (EDS; EDAX type: Sapphire). Analytical conditions of the SEM were: accelerating voltage, 15 kV; working distance, ~10 mm; counting time, 40 s. All mineralogical studies were carried out at the Institute of Earth Sciences, University of Silesia, Poland.

3. Results and discussion

3.1. Organic petrography

Organic matter present in the raw coals comprises macerals of vitrinite, liptinite, and inertinite groups following the terminology recommended by ICCP (1998, 2001) and Pickel et al. (2017). For description and identification of altered forms of organic matter in heated coals, the nomenclature employed by Kwiecińska and Petersen (2004) and Misz-Kennan et al. (2020), and discussed in Kus and Misz-Kennan (2017), was applied.

3.1.1. Raw samples

Contents of the vitrinite, liptinite, and inertinite maceral groups present in the raw-coal samples are typical for USCB coals (Zdanowski and Żakowa, 1995). Fusain, a product of wildfires affecting swamps (Taylor et al., 1998; ICCP, 2001; Scott and Jones, 1991; Scott and Glasspool, 2007; Richardson et al., 2012; Scott, 2000, 2018) was not observed macroscopically.

Vitrinite macerals were represented mainly by collotelinite, collodetrinite (Fig. 3a–d), and vitrodetrinite. Corpogelinite (Fig. 3a, b) and telinite with cells filled with resinite are rare. Inertinite macerals are usually fusinite (Fig. 3a, b, d), semifusinite (Fig. 3d), micrinite, inertodetrinite (Fig. 3a, b) and, much less commonly, funginite, macrinite and secretinite. Sporinite (Fig. 3a, b) and liptodetrinite are the most common liptinite macerals, while cutinite and resinite are rare. Some samples contain natural chars, porous or massive, pale grey to yellowish-white in colour, and characterised by a high reflectance (Fig. 3c). Coals M3 and M9 are substantially cracked, and coals G^1 and G^3 include some cracks (Fig. 3d).

Vitrinite is the dominant (56.4–79.4%) maceral group in coals collected in the Jankowice, Ziemowit, Wujek and Piekary coal mines. In two samples collected from Gołkowice core (G^3) and the Marcel mine (M11), vitrinite contents are also high (>70%). In other samples collected from these localities, vitrinite occurs in lesser amounts than liptinite- or inertinite-group macerals. Inertinite macerals (0.6–67.0%) are generally less abundant than vitrinite macerals. Only in M9, M12, and G^1 is the inertinite content greater than that of vitrinite (Table 2). Liptinite-maceral contents range from 0.4–12.6%. Natural chars are present (1.4%) in sample J3. In others (Z2, Z3, W4, W5), they are present, but their content is below the detection limit (< 0.2%). Mineral contents, mostly clay minerals and, in some cases, pyrite, are <22.2%

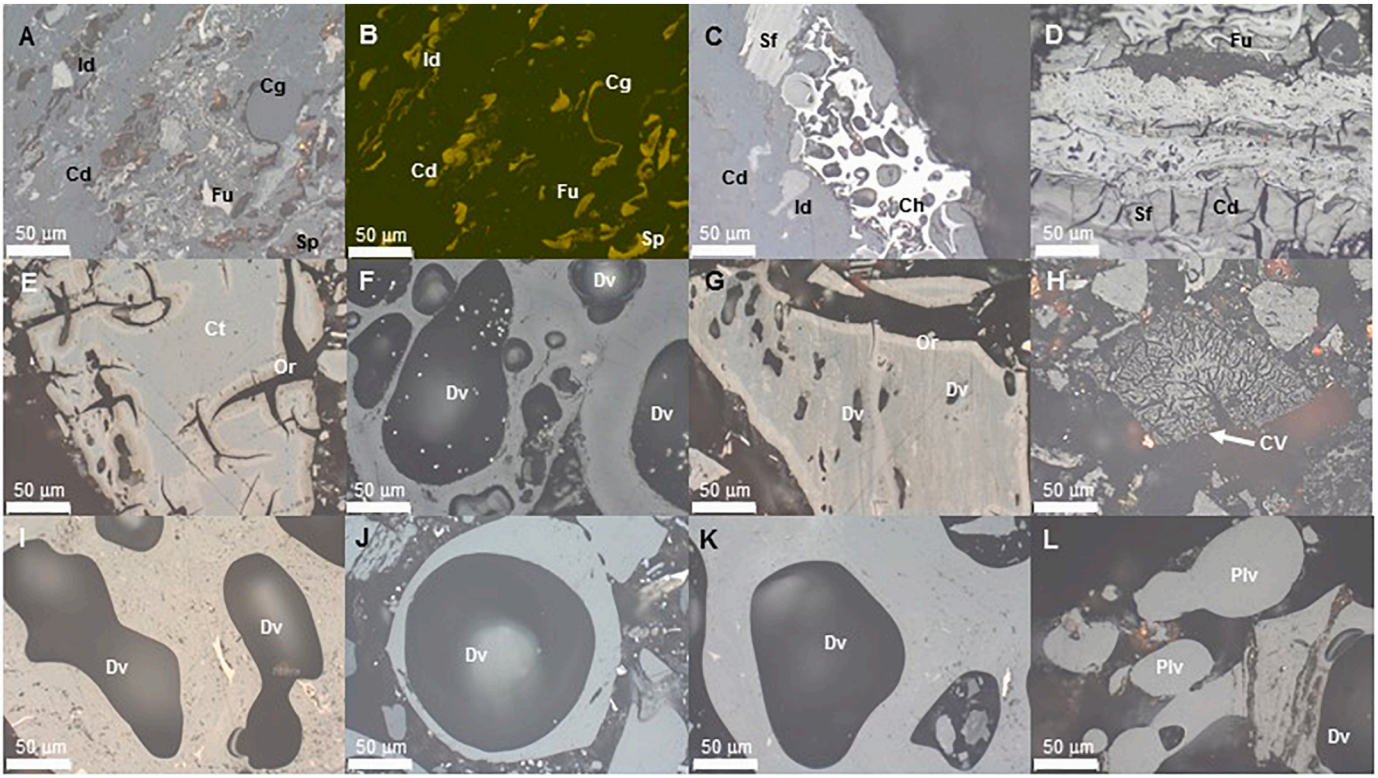

Fig. 3. Photomicrographs of organic matter in raw samples (A-D) and samples heated in semi-closed (*E*-H) and open (I-L) systems. A-B – collodetrinite (Cd), corpogelinite (Cg), sporinite (Sp), fusinite (Fu), inertodetrinite (Id); sample Z3. C – natural char (Ch), semifusinite (Sf), inertodetrinite, collodetrinite; sample J3. D – cracked semifusinite and collodetrinite, sample M3. E – brighter oxidation rims around irregular cracks in colotelinite (Ct) and devolatilisation pores (Dv), sample W4o. F – devolatilised organic matter particles; sample J3o. G – brighter-coloured oxidation rim (Or) around organic particle containing tiny devolatilisation pores; sample M12o. H – strongly cracked vitrinite (CV) particle; sample M3o. I-L– devolatilised- and plasticised vitrinite (Plv), samples G^1c, J4c, M11c and G^3c, respectively. Photomicrographs A, C-L – white light, B – fluorescence. Photographs by Magdalena Misz-Kennan.

(Table 2).

Coal-bearing rocks Gˆ2 and Mˆ7 are composed mainly of mineral matter (76.0 and 84.0%, respectively). Organic matter was dominated by liptinite in Mˆ7 and vitrinite in Gˆ2.

The random vitrinite reflectance (R_r) of the raw coals ranges from 0.56–0.99% and, in the raw coal-bearing rocks, 0.91–0.99%. Coals from the Piekary and Ziemowit mines are characterised by the lowest rank (R_r = 0.56–0.61%). That of coals from the other mines and core from Gołkowice is higher (0.72–0.99%).

3.1.2. Heated samples

Contents of organic matter in heated coals range from 0 to 99.8% (Table 2). In coals heated in the open system, contents fall within the range 0–99.8%, commonly <2%, and, in those heated in the semi-closed system, 23.8–99.8%, usually 96.2–99.8%. In samples obtained from semi-closed heating, minerals predominate only in samples Mˆ7c, Gˆ2c and Gˆ3c.

In general, organic matter is exposed to oxidation and the influence of temperature in both natural (e.g., Mastalerz et al., 2009; Kus, 2017a, 2017b) and industrial conditions (e.g., Suárez-Ruiz and Crelling, 2008; Suárez-Ruiz et al., 2019 and references therein). It undergoes alterations that are, the greater, the higher the temperature and the longer the heating time (Misz-Kennan and Fabiańska, 2010, 2011; Kus et al., 2017). The properties of organic matter, particularly maceral composition and rank, must also be taken into account (Misz-Kennan, 2010; Guo et al., 2020). Additionally, the presence/absence of air is also influencing the forms.

Heated coals show a great variety of morphological forms that reflect maceral composition and heating conditions (oxidised/pyrolytic, heating rate and time). Compared to vitrinite in unaltered coal, vitrinite with a paler grey colour exhibits a higher reflectance (e.g. Misz-Kennan, 2010; Misz-Kennan et al., 2020). Their colour is the paler and reflectance higher, the longer heating time. The impact of higher temperature is seen in plasticised particles that have rounded edges. Oxidation rims on particles have brighter colours and higher reflectance than unaltered particles (Misz-Kennan, 2010; Misz-Kennan and Fabiańska, 2011). Similar rims also occur around devolatilisation pores and cracks. Particles with round- or oval pores that range in size from a few to some tens of μm are related to the release of volatiles. Irregular internal cracks and fissures are another sign of temperature rise (Kus et al., 2017; Misz-Kennan et al., 2020). Strongly altered particles that are yellowish-white in colour and have much higher reflectance may reflect extended heated times (Misz-Kennan, 2010). The morphological features of some inertinite macerals (pyrofusinite, pyrosemifusinite, high reflectance macrinite) that do not change in the applied temperature range can still be seen (Goodarzi and Murchison, 1978; Murchison, 2006). For that reason, inertinite in altered particles is given a separate category here.

The reflectance of vitrinite in coals altered by semi-closed heating (1.23–2.02%) is somewhat lower than those altered by open-system heating (1.25–2.49%).

3.1.2.1. Open system. Particles heated in the open system are characterised by paler colours and higher reflectance compared to raw coals (Fig. 3e–h). Their typical feature is the presence of brightly-coloured oxidation rims observed around the external edge of some particles. Those rims also occur around irregular cracks and, sometimes, around devolatilisation pores (Fig. 3e–g). During heating in an open system, devolatilisation pores occur due to the release of volatile matter and the plasticity of organic particles (Fig. 3f–g). In some samples, irregular cracks are present within the particles, but in some, they are perpendicular to particle edges (Fig. 3e). The multiple cracks in sample M3o (Fig. 3h) are an extreme case. Another form typical for an open system is strongly altered organic matter of yellowish-white colour and high reflectance in some samples present in samples J3o, M11o, Gˆ1o, and Gˆ2o.

3.1.2.2. Semi-closed system. Particles heated in a semi-closed system also have a paler colour and higher reflectance than unaltered coals (Fig. 3i–l). Devolatilisation pores are a common feature of the heated particles in a semi-closed system (Fig. 3i–k). Some altered particles feature plasticised, rounded edges (Fig. 3l). The strongly altered organic matter with a yellowish-white colour and high reflectance was also present (J3c, M3c).

3.2. Mineral and chemical composition

Mineral matter present in samples of raw coal and coal-bearing rocks is consistent with the mineralogy of the pertinent part of the USCB (Klika and Kraussová, 1993; Muszyński et al., 2006; Parzentny, 2020); in the main, they comprise clay minerals such as kaolinite and illite, quartz, muscovite, chlorite, feldspars and accessory zircon, monazite and apatite. The presence of siderite, dolomite, pyrite, hematite and anatase, usually of sedimentary origin, was confirmed only by SEM-EDS (Fig. 4). However, they may be the result of thermal activity (veins, nests), as are ZnS (probably sphalerite), chalcopyrite, Na-alunite, barite, gypsum, halite, sylvite and elemental lead found in the samples (Fig. 4) though some may reflect weathering (Ward, 2002; Ward, 2016; Sokol et al., 2005; Stracher et al., 2011; Křibek et al., 2017; Finkelman et al., 2019).

The coals and coal-bearing raw samples' chemical composition differs in their ranges of major and trace elements (Table 3). In a qualitative sense, all detrital mineral matter should match in both. They differ quantitatively. Higher contents of SiO_2, TiO_2, Al_2O_3, Fe_2O_3, K_2O, Cr, Be, Sc, V, Ga, As, Rb, Y, Zr, Nb, Cs, Ba, rare earth elements (REEs), Hf, Ta, W, Th and U are due to the abundance of rock-forming minerals in coal-bearing rocks. Secondary natroalunite, gypsum, barite, celestine, Fe sulphides and oxides underpin higher contents of Na_2O, CaO, Fe_2O_3, Ba and Sr. Zinc, Pb, As and Cu also form their own mineral phases (Fig. 4d). However, higher contents of almost all trace elements in coal-bearing samples signify that most derived from mineral matter and not from organic matter, apart from mercury and REEs which concentration is also increased in coal samples (Table 3; Dai et al., 2016; Seredin and Dai, 2012; Ward, 2002).

3.3. Organic geochemistry

Extract yields are variable: 1.5–3.8 wt% for raw coals, very low (~ 0.05 wt%) for samples heated in the open system and higher (< 6.2 wt %) for those heated in the semi-closed system (Table 1). In the open system, any bitumen in the coals formed due to heating was freely expelled and evaporated, whereas in the semi-closed system, the pyrolysate formed was adsorbed within the rock, increasing its extractability.

3.3.1. Raw samples

The organic geochemistry of raw coal-bearing rocks and bituminous coal varies widely, depending on sample maturity and possible heating influence. Both coals from the Ziemowit mine (Z1 and Z2) were at the beginning of catagenesis, with Carbon Preference Index (CPI) values for *n*-alkanes of ~1.5 and 17β,21α(H)-hopanes (abbreviated as βα hopanes, or moretanes) present in relatively high amounts with a ratio of βα/(αβ + βα) hopanes of 0.43. The ratio of 17α(H),21β(H)-homohopane 20S to the sum of 20S and 20R diastereomers is approximately 0.35; Ts/(Ts + Tm) is ~0.7, indicating a low level of thermal maturity. Methyl phenanthrene indices MPI-1 and MPI-3 are ~0.60 and ~ 0.71, respectively. The pristane/phytane ratio (Pr/Ph) is high, as in the case of most humic coals, since there was input from sources other than chlorophyll, e.g., α-tocopherol (Goossens et al., 1984).

The raw samples from the Marcel and Jankowice mines (Mˆ7, M11, M12, J3, J4) are much more mature – no earlier than in mid-catagenesis. CPI values close to 1.1, small amounts of moretanes, and C_{31}20S/(20S + 20R) values of ~0.57 indicate the limit of the ratio utility since mid-catagenesis had been reached. MPI-1 and MPI-3 values are higher at

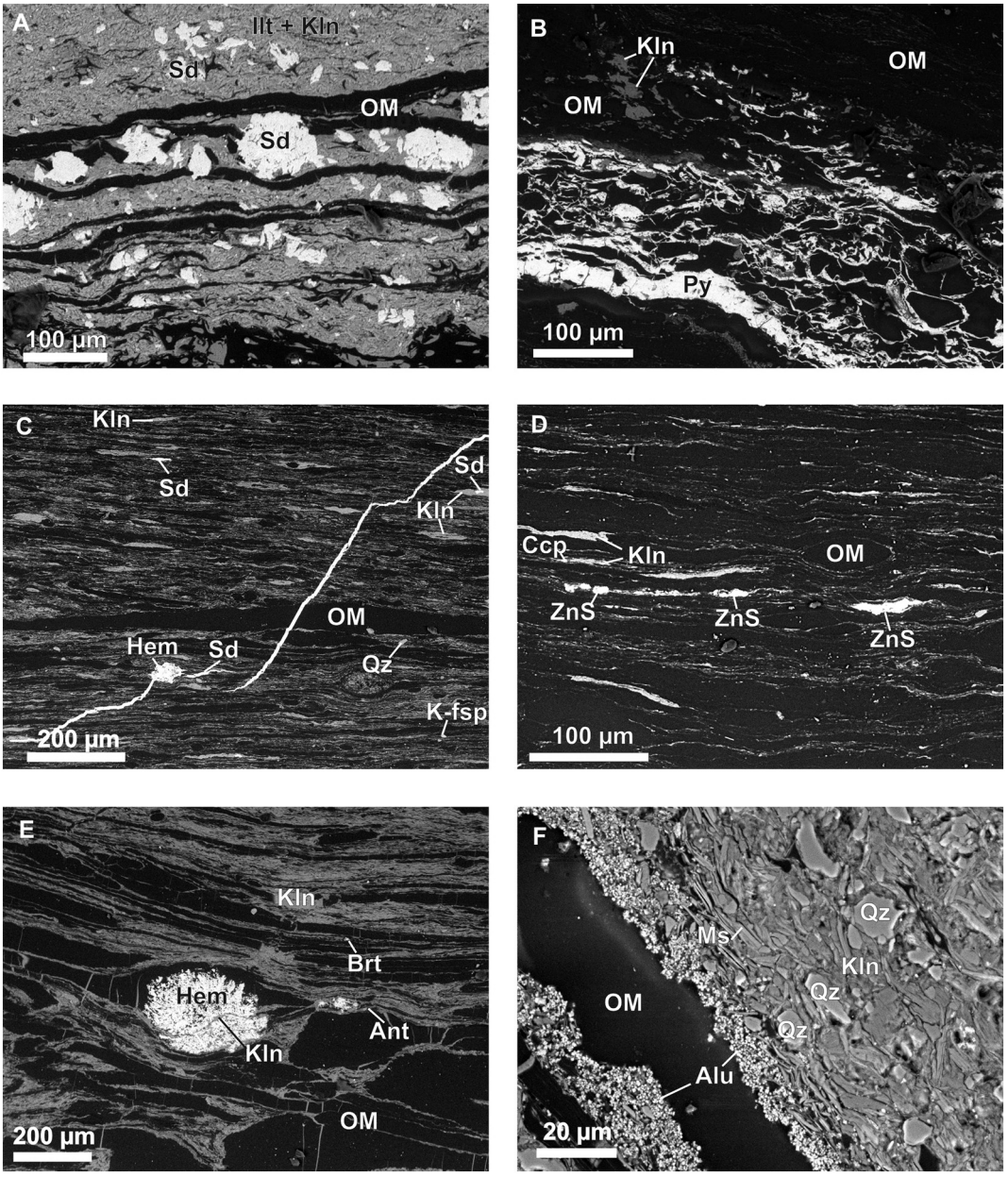

Fig. 4. BSE images of mineral matter in raw samples thought to have been affected by heating in the geological past. A – siderite (Sd) crystallised within barren rocks composed of kaolinite (Kln), illite (Ilt) and organic matter (OM); sample Gˆ2. B – Pyrite (Py) veins and kaolinite in coal; sample Gˆ1. C – siderite vein cutting barren-rock composed of kaolinite, quartz (Qz), K-feldspar (K-fsp), siderite and organic matter; sample Gˆ3. D – Sphalerite? (ZnS) and chalcopyrite (Ccp); sample Gˆ3. E – Hematite (Hem), barite (Brt), anatase (Ant) and kaolinite in coal; sample J3. F – Na-alunite (Alu) crystallising within a barren rock composed of quartz, kaolinite and muscovite (Ms) along a coal vein; sample Mˆ7. Photographs by Justyna Ciesielczuk.

0.91 and 0.91 (average), respectively. Increased maturity is shown by samples M3 and M9. The Wujek and Piekary coals (W5 and P5) exhibit features between these two extremes. The organic geochemistry results accord with the known thermal history of the USCB and the trend of coal rank within the basin described in the literature (Gabzdyl et al., 1997; Gabzdyl and Probierz, 1987; Jureczka and Kotas, 1995; Jureczka et al., 2005; Martinec et al., 2005).

Special attention was paid to the geochemistry of the Gołkowice core and the Marcel M3 and M9 samples, as earlier heating within the deposit was suspected. One of the features suggesting such is the almost two times decrease in volatile contents in most of them compared to the other investigated samples and bituminous coals of this region (Table 1). This could be due to the escape of the lightest compounds during intradeposit heating. The Gˆ1–Gˆ3 raw-rock extracts contain large amounts of light hydrocarbons (Figs. 5 and 6), which may reflect thermal stress and release of lighter compounds from the macromolecule. If so, the system was closed, as these heating products did not migrate to the surrounding rocks and may have been captured by mainly clay minerals and organic matter. Samples M3 and M9 exhibit no such features, though the smooth *n*-alkane outline with a Gaussian shape suggests heating within the deposit and migration of pyrolytic products to the surrounding rocks.

3.3.2. *Heated samples*

3.3.2.1. Open system. The laboratory open-system heating experiment, with free access to oxygen and free evaporation of organic compounds, led to the almost total destruction of bitumen, either free or bound with

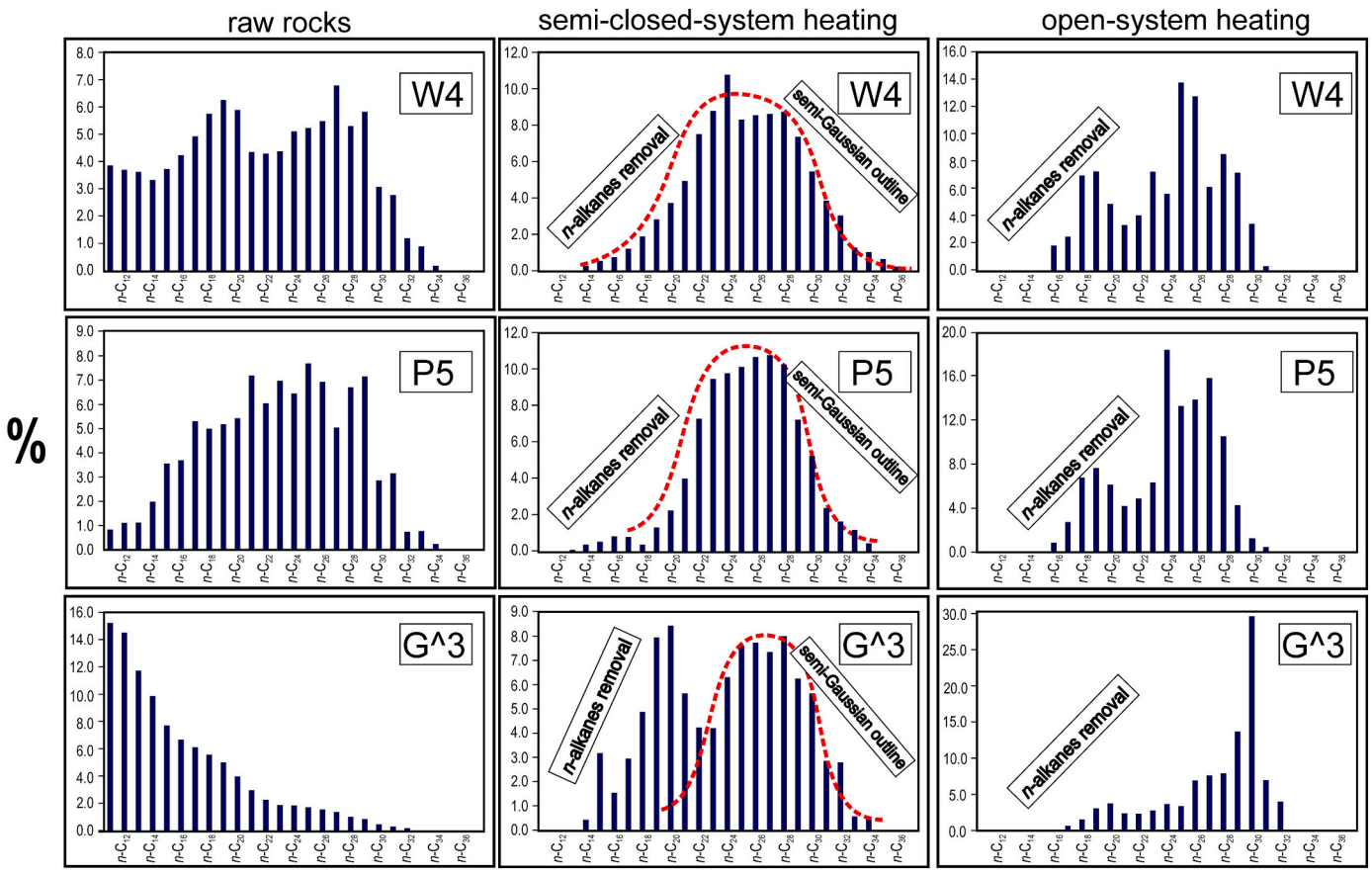

Fig. 5. Comparison of *n*-alkane distribution profiles.

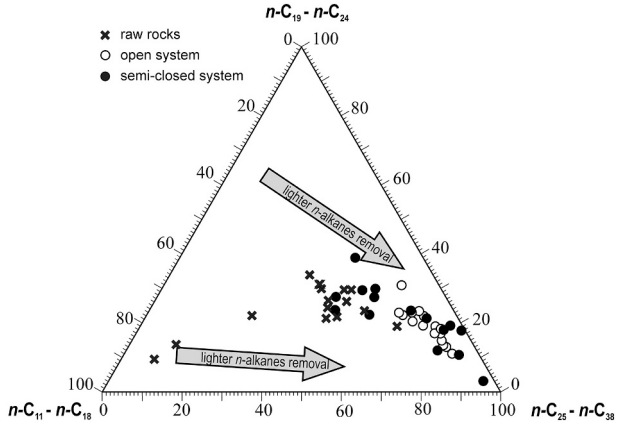

Fig. 6. The shift in relative percentage contents of light (*n*-C_{11}-*n*-C_{18}), intermediate (*n*-C_{19}-*n*-C_{24}) and long-chain (*n*-C_{15}-*n*-C_{38}) *n*-alkanes caused by different heating conditions.

a macromolecule. Lightweight compounds were evaporated or oxidised. Tiny amounts of residual bitumen are composed predominantly of heavy PAHs and their oxidised products. Such compositional changes are shown by a significant depletion of the bituminous fraction in lighter compounds such as *n*-alkanes, alkyl biphenyls, alkyl naphthalenes, and even alkylphenanthrenes (Fig. 7). The distribution of *n*-alkanes changed from bimodal, common in terrestrial organic matter, to pyrolytic – to the Gaussian outline (Fig. 5). Carbon Preference Index (CPI) values decreased slightly. However, this decrease was not very pronounced as organic matter in USCB Pennsylvanian coals and shales is mature and commonly exhibits CPI values of ~1.2–1.5 (Fabiańska et al., 2013). The distribution of *n*-alkanes is significantly depleted in lighter compounds (Fig. 5), as shown by Σ2/Σ1 (the ratio of long-chain (*n*-C_{23}-*n*-C_{37}) to short-chain (*n*-C_{11}-*n*-C_{22}) *n*-alkanes), values of ~3.0–4.5 (Table 4). Relative percentage contents of lighter *n*-alkanes in the range *n*-C_{11}-*n*-C_{18} decreased from ~25–35% (relative) for most coal samples and from ~80% for Gołkowice IV core samples to ~5–15% (relative) (Fig. 6). The lesser degree of *n*-alkane removal is also reflected by an approximately twofold increase in Σ2/Σ1 values. Pristane-to-phytane (Pr/Ph) values decreased from ~3–7, a range characteristic of most humic bituminous coals of the USCB, to ~0.5; pristane removal predominated over phytane removal (Table 4; Fabiańska et al., 2013). As Pr is one carbon atom lighter than Ph, it evaporated more readily from heated samples; Pr and Ph's boiling temperatures are 296 and 322.41 °C at 760 mmHg, respectively (ChemSrc, 2021). Pr/*n*-C_{17} significantly decreased in most open-system heated samples, except for G^2, G^3 and W4, in which this ratio showed a slight increase. However, Ph/*n*-C_{18} in all samples increased slightly from ~0.3–0.5 to ~0.5–0.7, possibly due to the preferential removal of *n*-octadecane with a boiling point of 316.3 °C at 760 mmHg (PubChem).

The only high-molecular-weight compounds removed from most open-heated samples were pentacyclic triterpanes (hopanes and moretanes), possibly due to their low thermal resistance level. Open-system heating favours the removal of naphthalene due to its low boiling point (ChemSpider, 2021, ChemSrc, 2021). Due to oxic conditions, PAHs' formation, such as anthracene or indeno[1,2,3-cd] pyrene related to combustion, is favoured (Radke, 1987). This reduced values of the ratio of phenanthrene to anthracene approximately two- to fourfold (P/A in Table 5) and increased values of the ratio of indeno[1,2,3-cd] pyrene to benzo[*ghi*]perylene when these compounds occurred in extracts from the M3 and J4 samples (Id/(BghiPer+Id) in Table 5). A trend similar to that observed in non-substituted PAHs could be seen in distributions of

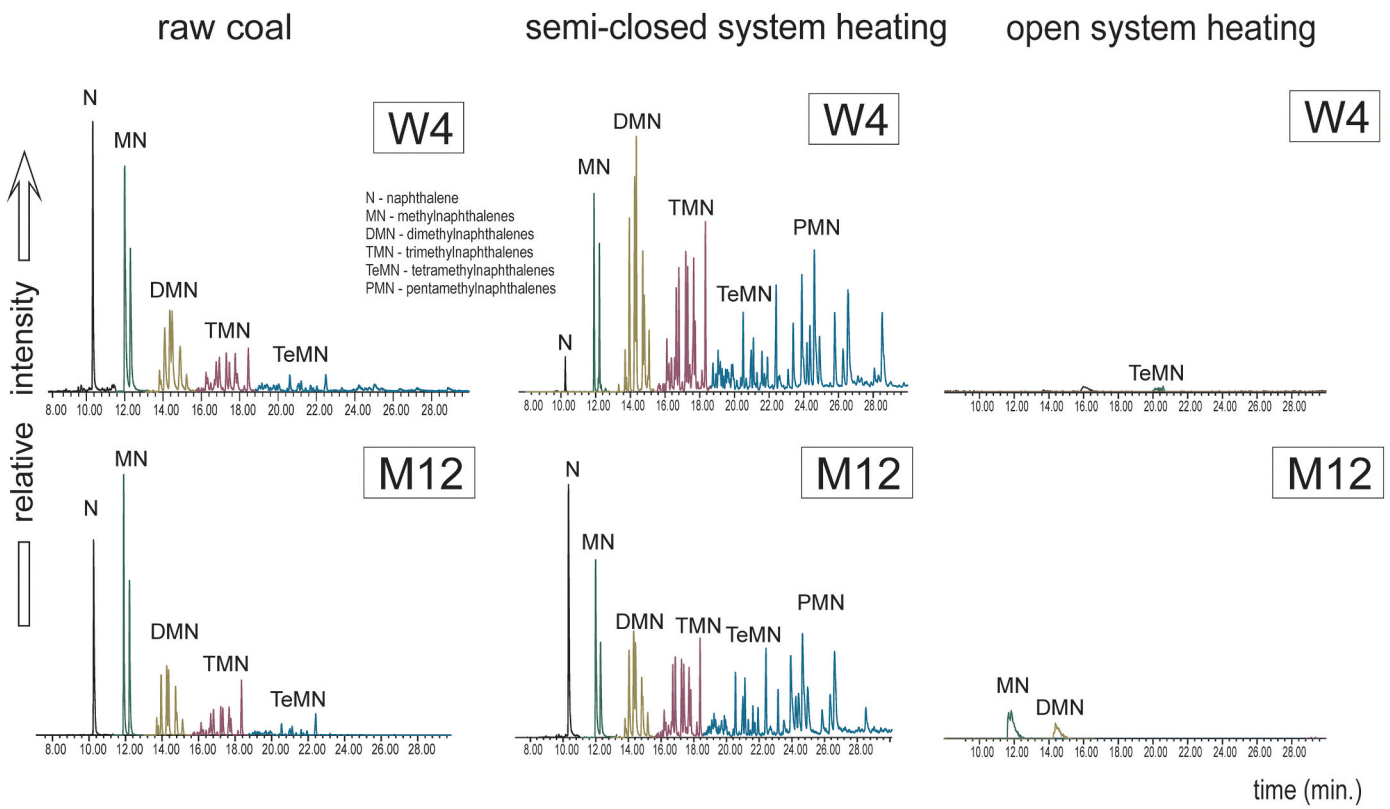

Fig. 7. Changes in the distribution of naphthalene and its C_1-C_5 alkyl derivatives caused by different heating conditions.

alkyl aromatic hydrocarbons when raw samples were compared with those from open-system heating (Fig. 7). Most of these compounds – in particular alkyl naphthalenes and alkyl biphenyls, as the most volatile, were removed during open-system heating. Their removal and the light aliphatic hydrocarbons led to changes in carbon isotope distribution.

It seems that, with open-system heating, the main deciding factor in aliphatic- compound removal is the boiling point of a given compound. The sorptive properties of the organic- and mineral fraction play a minor role. In the case of aromatic hydrocarbons, an additional factor changing ratio values is sorption, as these compounds exhibit higher polarity than non-polar aliphatic hydrocarbons and thus a greater affinity for the inorganic matrix.

3.3.2.2. Semi-closed system. A semi-closed-system heating experiment with oxygen depletion increased extract yields in comparison to those of raw coals and coal-bearing rocks. The extracts were enriched in bitumen due to closed pores and, possibly, partial pyrolysis of organic matter. However, typical pyrolytic products such as *n*-alken-1-es were not found in the extracts, indicating a temperature was too low or a time too short to allow advanced macromolecule cracking. Most lighter compounds are still present in these extracts, preserving the compounds' initial distributions and ratios. Increases in *n*-alkane concentrations over Pr and Ph and aromatic hydrocarbons over aliphatic hydrocarbons are the most significant composition changes in these samples. Thus, Pr/*n*-C_{17} and Ph/*n*-C_{18} values mainly decreased, and their points shifted in the Shanmugam diagram to the area corresponding to more mature samples (Shanmungam, 1985). The exceptions are samples (M3, Mˆ7 and Gˆ1–Gˆ3) supposedly heated within a deposit; these show much lower changes in ratio values or even opposite trends.

In the samples from semi-closed-system heating, alkyl aromatic hydrocarbons were mostly retained with, however, altered relative contents (Fig. 7). Contents of naphthalene and methyl naphthalenes decreased, whereas tetra- and pentamethyl naphthalenes increased in relative contents. This effect, deriving from lighter compounds' evaporation, is limited compared to open-system heating, though it still affects composition.

Alkyl naphthalene ratios are affected by heating to the same extent (Table 4). Their values may be modified in two ways. Firstly, isomers of alkyl aromatic hydrocarbons show various thermal resistance degrees; maturity indices such as the methyl naphthalene ratio (MNR) and methyl phenanthrene indices (MPI-1 and MPI-3) are based on this phenomenon. The ratios are constructed such that their values increase linearly with increasing expression of maturity, e.g., vitrinite reflectance. However, when the ratio's maximal value is achieved, more thermally resistant alkyl isomers start to decay, and the ratio values decrease (Radke and Welte, 1983). This can explain seemingly erratic changes in dimethylnaphthalene ratio (DNR) values. Since more mature samples have already achieved high DNR values, i.e., approached the end of ratio utility, DNR values will decrease on heating. Less mature samples, such as the coals from the Ziemowit mine, continue to show increases in DNR values on heating. MPI-3 and MPI-1 values mainly increased following semi-closed-system heating, possibly due to these indices' wider utility range. No change or decrease in these values was seen in samples that were already mature or had possibly been heated within a deposit (Gˆ1–3 rocks and M3, Mˆ7 and M9). The Marcel samples (M11 and M12), which were not affected by intra-deposit heating, showed an expected increase in ratio values following semi-closed-system heating. Thus, it can be assumed that significant discrepancies between vitrinite reflectance values and between several alkyl aromatic hydrocarbon ratios much more heating sensitive reflect thermal effects, which differ from those associated with normal thermal evolution within a deposit. DNR appears to be the best ratio for detecting such changes.

Ratio values based on alkyl aromatic hydrocarbons are also affected by differences between the boiling points of particular isomers of alkyl aromatic hydrocarbons, in particular in open-system heating, but also in semi-closed-system heating, e.g., the boiling point of 1-methyl naphthalene is 242 °C, that of 2-methylnaphthalene 241 °C (ChemSpider,

Table 4
Values of geochemical biomaker ratios for raw samples and for samples heated in open (o) and semi-closed (c) systems.

Sample No	Σ2/Σ1 1)	CPI 2)	Pr/Ph 3)	Pr/*n*-C_{17} 4)	Ph/*n*-C_{18} 5)	Ts/(Tm + Ts) 6)	C_{30}βα/ (αβ + βα) 7)	C_{31}S/ (S + R) 8)	C_{29}Ts/ (C_{29} + C_{29}Ts) 9)
J3	0.87	0.96	3.59	0.94	0.27	0.75	0.25	0.38	0.05
J3o	1.99	1.24	0.49	0.37	0.47	–	–	–	–
J3c	1.52	1.13	3.25	0.96	0.24	0.93	0.21	0.60	0.02
J4	0.95	1.18	4.00	0.56	0.13	0.93	0.19	0.58	0.06
J4o	4.08	1.03	0.56	1.25	0.30	–	–	–	–
J4c	1.04	1.07	4.43	0.74	0.23	0.88	0.27	0.64	0.05
M3	0.72	1.35	6.27	1.34	0.31	0.90	0.34	0.60	0.00
M3o	3.07	1.11	0.37	1.17	0.48	–	–	–	–
M3c	1.58	1.16	2.77	0.92	0.25	0.84	0.37	0.58	0.01
Mˆ7	0.94	1.14	5.63	1.54	0.37	0.92	0.28	0.55	0.01
Mˆ7o	3.04	1.07	0.36	1.23	0.48	–	–	–	–
Mˆ7c	4.70	1.55	4.36	1.46	0.25	0.74	0.28	0.33	0.01
M9	0.83	1.12	6.78	1.43	0.24	0.89	0.34	0.59	0.00
M9o	3.97	0.96	0.32	0.92	0.48	–	–	–	–
M9c	4.44	1.30	2.06	0.52	0.09	0.78	0.38	0.49	0.13
M11	1.06	0.97	3.99	1.62	0.38	0.90	0.24	0.58	0.05
M11o	3.31	1.14	0.46	0.95	0.73	0.75	0.43	0.57	0.19
M11c	3.42	1.08	2.32	0.43	0.11	0.87	0.29	0.57	0.71
M12	0.78	1.19	7.11	3.16	0.42	0.93	0.24	0.57	0.03
M12o	3.12	0.94	0.58	1.24	0.77	0.82	0.46	0.45	0.14
M12c	9.63	0.98	2.39	1.02	0.32	0.80	0.31	0.57	0.02
Z2	1.23	1.54	5.11	4.24	0.66	0.69	0.42	0.33	0.05
Z2o	1.95	1.05	0.44	0.93	0.64	0.65	0.37	0.45	0.14
Z2c	0.94	1.33	0.92	1.04	0.70	–	–	–	–
Z3	2.08	1.25	2.78	2.70	0.80	0.73	0.43	0.37	0.03
Z3o	4.06	1.12	0.38	1.00	0.68	0.52	0.19	0.44	0.10
Z3c	1.12	1.05	2.32	0.42	0.14	0.62	0.53	0.37	0.04
W4	1.01	1.26	1.44	0.37	0.22	0.82	0.39	0.55	0.02
W4o	2.54	1.00	0.60	1.12	0.69	0.75	0.25	0.53	0.13
W4c	5.37	0.96	4.05	0.26	0.04	0.80	0.37	0.54	0.01
W5	0.96	1.18	5.22	2.94	0.52	0.93	0.24	0.59	0.03
W5o	2.27	0.90	0.80	1.19	0.71	0.85	0.35	0.54	0.10
W5c	2.32	1.08	1.99	1.22	0.50	0.89	0.29	0.57	0.02
P5	1.48	1.15	4.30	3.24	0.80	0.64	0.41	0.38	0.03
P5o	2.60	1.50	0.54	1.04	0.77	0.78	0.40	0.49	0.12
P5c	7.31	0.99	0.89	1.25	2.86	0.63	0.51	0.31	0.01
Gˆ1	0.39	1.24	4.37	1.10	0.25	0.79	0.15	0.60	0.18
Gˆ1o	4.20	0.89	0.47	0.78	0.65	0.81	0.30	0.57	0.10
Gˆ1c	13.03	0.98	2.65	1.29	0.28	0.77	0.19	0.58	0.11
Gˆ2	0.10	1.04	2.67	0.42	0.21	–	–	–	–
Gˆ2o	2.72	0.93	0.44	0.87	0.68	0.89	0.34	0.58	0.11
Gˆ2c	1.29	1.18	1.28	1.17	0.56	–	–	–	–
Gˆ3	0.16	1.08	2.95	0.72	0.27	–	–	–	–
Gˆ3o	6.45	1.61	0.62	0.97	0.69	0.50	0.40	0.52	0.17
Gˆ3c	1.54	1.22	0.81	0.86	0.66	0.85	0.31	0.72	0.02

1) Σ2/ Σ 1 = [Σ(from *n*-C_{23} to *n*-C_{37})]/[Σ (from *n*-C_{11} to *n*-C_{22})]; *m/z* = 71, source indicator (Tissot and Welte, 1984).
2) CPI =0.5{[(*n*-C_{25} + *n*-C_{27} + *n*-C_{29} + *n*-C_{31} + *n*-C_{33})/(*n*-C_{24} + *n*-C_{26} + *n*-C_{28} + *n*-C_{30} + *n*-C_{32})] + [(*n*-C_{25} + *n*-C_{27} + *n*-C_{29} + *n*-C_{31} + *n*-C_{33})/(*n*-C_{26} + *n*-C_{28} + *n*-C_{30} + *n*-C_{32} + *n*-C_{34})]; Carbon Preference Index; *m/z* = 71; thermal maturity parameter (Bray and Evans, 1963).
3) Pr/Ph = pristane/phytane; parameter of environment oxicity (with exception of coals); *m/z* = 71 (Didyk et al., 1978).
4) Pr/*n*-C_{17} = pristane/*n*-heptadecane; *m/z* = 71 (Leythauser and Schwartzkopf, 1985).
5) Ph/*n*-C_{18} = phytane/*n*-octadecane; *m/z* = 71 (Leythauser and Schwartzkopf, 1985).
6) Ts/(Ts + Tm) = 18α(H)-22,29,30-trisnorneohopane/(18α(H)-22,29,30-trisnorneohopane+17α(H)-22,29,30-trisnorhopane); *m/z* = 191; thermal maturity parameter (Seifert and Moldowan, 1986).
7) C_{31}S/(S + R) = 17α(H),21β(H)-29-homohopane 22S/(17α(H),21β(H)-29-homohopane 22S + 17α(H),21β(H)-29-homohopane 22R); *m/z* = 191; thermal maturity parameter (Seifert and Moldowan, 1986).
8) C_{30}βα/(αβ + βα) = 17β(H),21α(H)-29-hopane C_{30}/(17α(H),21β(H)-29-hopane C_{30} + 17β(H),21α(H)-29-hopane C_{30}); *m/z* = 191 (Seifert and Moldowan, 1986).
9) C_{29}Ts/(C_{29} + C_{29}Ts) = 18α(H)-30-norneohopane/(17α(H),21β(H)-29-homohopane +18α(H)-30-norneohopane); *m/z* = 191 (Peters et al., 2005).
"–" compounds not detected; or compounds detected but concentrations too low to calculate a parameter value.

2021, ChemSrc, 2021). The difference appears small, but given the likely duration of intra-deposit heating, ratio values may significantly be impacted.

With semi-closed-system heating, the picture is not as simple as with open-system heating, in which the main factor is the boiling temperature of a given compound. Here, several factors affecting geochemical ratio values should be considered. Among these factors is coal rank as the sample set covered a relatively wide range of thermal maturity, from the initial- (the Ziemowit samples, R_r = 0.56%) to the advanced stages of catagenesis. Samples Gˆ1–Gˆ3, M3, and Mˆ7 were probably also heated by an intradeposit fire that changed their initial geochemical properties to much more mature ones. In addition to organic-matter maturity, another significant factor is the presence of clay minerals, e.g., in the coal shale Mˆ7. Clay minerals adsorb components of pyrolysate/pore bitumen which are much stronger than organic matter itself. Another factor is coal petrography. Liptinite macerals tend to expel more bitumen and more aliphatic compounds than vitrinite macerals; the former tend to produce aromatic hydrocarbons.

The question that arises from the organic geochemistry investigation is whether the Jankowice samples (J3 and J4) were affected by the intra-

Table 5
Values of aromatic hydrocarbon indices for raw samples and for samples heated in open (o) and semi-closed (c) systems.

Sample no	MNR 1)	DNR-1 2)	MPI-3 3)	MPI-1 4)	Rc 5)	MP/P	P/A	A/(A + P)	Fl/(Fl + Py)	Fl/(Fl + P)	BaA/(BaA + Ch)	BaP/BghiP	IP/(IP + BghiP)
J3	1.58	4.77	1.11	0.94	0.96	1.26	25.08	0.04	0.37	0.06	0.46	2.20	0.21
J3o	1.44	16.28	0.84	0.62	0.77	0.89	7.50	0.12	0.60	0.44	0.88	–	–
J3c	0.78	2.21	0.79	0.93	0.96	1.98	7.12	0.12	0.31	0.12	0.33	1.73	0.17
J4	0.67	2.72	0.97	0.98	0.99	1.61	34.23	0.03	0.29	0.08	0.32	2.10	0.16
J4o	1.81	–	0.91	1.06	1.03	2.03	4.48	0.18	0.51	0.51	0.35	1.03	0.41
J4c	1.63	7.29	0.93	0.97	0.98	1.68	5.26	0.16	0.39	0.15	0.48	1.98	0.26
M3	1.42	2.83	1.88	1.56	1.34	1.69	6.59	0.13	0.66	0.91	0.45	1.52	0.43
M3o	1.52	3.89	0.65	0.53	0.72	0.95	3.35	0.23	0.44	0.28	0.27	0.62	0.70
M3c	2.12	1.53	1.27	0.73	0.84	0.78	1.39	0.42	0.50	0.33	0.50	3.14	0.42
M^7	0.90	2.71	0.88	0.86	0.92	1.45	26.66	0.04	0.45	0.14	0.47	1.78	0.20
M^7o	1.65	3.26	1.09	1.03	1.02	1.50	2.34	0.30	0.59	0.46	0.23	–	–
M^7c	1.48	3.00	1.20	0.70	0.82	0.77	2.55	0.28	0.40	0.24	0.49	4.02	0.27
M9	1.40	2.00	1.70	2.09	1.66	3.27	13.71	0.07	0.62	0.90	0.49	2.42	0.41
M9o	1.45	21.70	0.70	0.57	0.74	0.97	5.09	0.16	0.48	0.30	0.28	–	–
M9c	3.12	1.67	1.14	0.58	0.75	0.63	1.85	0.35	0.42	0.25	0.53	2.65	0.29
M11	0.26	2.11	0.87	0.99	0.99	1.90	14.57	0.06	0.41	0.14	0.19	3.62	0.45
M11o	–	–	–	–	–	–	5.19	0.16	–	–	–	–	–
M11c	1.72	2.13	0.93	1.21	1.13	2.63	1.86	0.35	0.32	0.23	0.53	4.47	0.29
M12	1.46	3.60	0.78	0.81	0.88	1.52	35.15	0.03	0.39	0.10	0.26	2.82	0.27
M12o	–	–	–	–	–	–	14.43	0.06	–	–	–	–	–
M12c	1.91	3.09	1.09	1.47	1.28	3.10	2.22	0.31	0.31	0.47	0.52	2.65	0.36
Z2	1.22	1.54	0.68	0.66	0.80	1.28	3.73	0.21	0.60	0.47	0.52	3.03	0.56
Z2o	–	–	1.73	1.10	1.06	–	6.99	0.13	0.30	0.45	0.50	–	–
Z2c	0.90	2.84	0.57	0.71	0.82	1.94	2.46	0.29	0.47	0.43	0.33	32.52	0.68
Z3	1.12	1.28	0.75	0.56	0.74	0.88	2.65	0.27	0.63	0.54	0.53	2.06	0.53
Z3o	–	–	–	–	–	–	6.46	0.13	0.24	0.45	0.61	–	–
Z3c	1.41	2.63	1.06	1.32	1.19	2.57	5.15	0.16	0.35	0.11	0.36	4.90	0.38
W4	1.63	2.08	0.73	0.97	0.98	2.47	1.11	0.47	0.36	0.30	0.51	1.39	0.36
W4o	–	–	–	–	–	–	–	–	–	–	–	–	–
W4c	1.33	1.54	1.02	1.43	1.26	3.32	0.74	0.57	0.36	0.41	0.62	2.40	0.41
W5	1.12	–	0.86	0.73	0.84	1.13	14.58	0.06	0.42	0.11	0.42	2.01	0.33
W5o	–	–	1.37	1.06	1.03	–	6.71	0.13	0.35	0.31	0.46	–	–
W5c	1.24	1.57	0.73	0.77	0.86	1.51	4.39	0.19	0.40	0.14	0.41	3.71	0.37
P5	–	–	0.89	0.86	0.92	1.42	3.29	0.23	0.22	0.47	0.33	1.73	0.43
P5o	–	–	–	–	–	–	–	–	–	–	–	–	–
P5c	1.71	3.28	1.05	0.97	0.98	1.43	1.23	0.45	0.37	0.38	0.48	2.09	0.43
G^1	0.52	2.60	1.08	1.28	1.17	2.30	–	–	0.35	0.09	0.26	4.22	0.29
G^1o	–	–	–	–	–	–	8.71	0.10	0.58	0.96	0.63	–	–
G^1c	1.25	1.30	1.22	1.25	1.15	1.87	2.67	0.27	0.27	0.43	0.48	10.30	0.39
G^2	0.93	2.34	1.04	1.10	1.06	1.81	20.74	0.05	0.50	0.09	0.49	–	–
G^2o	–	–	–	–	–	–	3.09	0.24	0.39	0.81	0.61	–	–
G^2c	1.63	9.93	0.99	1.05	1.03	1.77	3.39	0.23	0.40	0.22	0.36	2.07	0.35
G^3	0.75	4.76	1.28	1.13	1.08	1.48	–	–	0.30	0.02	0.11	0.19	0.09
G^3o	–	–	0.88	0.77	0.86	–	5.08	0.16	0.58	0.83	–	–	–
G^3c	1.72	7.11	1.07	1.21	1.13	2.09	2.35	0.30	0.34	0.15	0.45	2.35	0.36

1) MNR = 2-methylnaphthalene/1-methylnaphthalene; $m/z = 142$; thermal maturity parameter (Radke, 1987).
2) DNR-1 = (2,6-dimethylnaphthalene +2,7- dimethylnaphthalene)/1,5-dimethylnaphthalene; $m/z = 156$, thermal maturity parameter (Radke, 1987).
3) MPI-3 = (2-methylphenanthrene+3-methylphenanthrene)/(1-methylphenanthrene+9-methylphenanthrene); $m/z = 192$; thermal maturity parameter (Radke and Welte, 1983).
4) MPI-1 = (2-methylphenanthrene+3-methylphenanthrene)/(phenanthrene+1-methylphenanthrene+9-methylphenanthrene); $m/z = 192$; thermal maturity parameter (Radke and Welte, 1983).
5) $R_c = 0.60$ MPI-1 + 0.40; calculated according to the Radke's formula (1987).
Abbreviations: A - anthracene, BaA - benzo(*a*)anthracene, BaP - benzo(*a*)pyrene, BghiP - benzo(*ghi*)perylene, Ch - chrysene, F - fluoranthene, IP - indeno[1,2,3,-*cd*] pyrene, P - phenanthrene, Py - pyrene,
"–" compounds not detected; or compounds detected but concentrations too low to calculate a parameter value.

deposit fire. The sampling site is sufficiently close to the suspected zone of heating. The organic matter in these samples shows some signs of heating, e.g., the smooth outline of their *n*-alkane distribution indicative of pyrolytic heating without oxygen access and some depletion in lighter compounds (Figs. 5 and 6). Moreover, there was no decrease, as in other samples, in the J3 ratios of alkyl aromatic hydrocarbons following semi-closed-system heating, whereas the J4 values show random increases/decreases.

3.4. Carbon isotope composition

3.4.1. Raw samples

The $\delta^{13}C_{TC}$ values for raw coals and coal-bearing rocks, the percentage of total carbon contributions (TC), and the same data for experimentally heated samples are reported in Table 1. The carbon percentage varies over a wide range from 39.1–84.6% in raw coals and from 8.1–26.3% in coal-bearing rocks. The $\delta^{13}C_{TC}$ values for coal samples range from −24.51‰ to −22.07‰ (average − 23.26 ± 0.67‰, median − 23.27‰; Table 1). The similar average- and median values reflect a narrow spread of values and enable the use of the average value of $\delta^{13}C_{TC}$ as representative of the coal sample-group. The $\delta^{13}C_{TC}$ values for coal-bearing rocks range from −23.05‰ to −22.12‰ (average − 22.59 ± 0.46‰).

The $\delta^{13}C_{TC}$ values for the raw coal and raw coal-bearing rocks indicate that these are slightly more enriched in ^{13}C than data in the literature. Kotarba and Clayton (2003) reported $\delta^{13}C_{TC}$ values for USCB

coals ranging from −24.5 to −23.2‰ (average − 23.9 ± 0.3‰) and, for USCB coal shales, from −24.2 to −22.4‰ (average − 23.6 ± 0.5‰). The differences between our data and those of Kotarba and Clayton (2003) may be explained by (i) the different coal seam sampled for our study (Fig. 2) and (ii) variability in isotope- and maceral composition within the same coal/shale bed (see Fig. 2). Different maceral contents can influence the final isotopic signal (Rimmer et al., 2006). For instance, the $\delta^{13}C$ of cellulose, a major wood component, may be enriched in ^{13}C by 1–2‰ compared to the whole wood tissue, whereas lignin, another major component, may be depleted in ^{13}C by 2–6‰ (Benner et al., 1987; Bird and Ascough, 2012). Thus, even a slight difference in the petrographic composition can lead to a different total carbon isotopic signal.

The differences between mineralogical and geochemical parameters between coal and coal-bearing rocks manifest in differences in $\delta^{13}C_{TC}$ in both groups, similar to Rahman et al. (2018). Hence, we expected a different geochemical-mineralogical-isotopic response for both analysed groups during our experiments.

3.4.2. Heated samples

The actual geochemical conditions during the intradeposit fire that may have affected the investigated rocks are unknown; therefore, both open (with sufficient O_2) and semi-closed (without gaseous O2) molar conditions were tested.

Coal samples heated in the open system show a wide TC range from 0.3–74.8% and a wide range of $\delta^{13}C_{TC}$ values from −23.29 to −12.71‰, whereas samples from the semi-closed system have TC values ranging from 35.7 to 84.5% and $\delta^{13}C_{TC}$ values characterised by a distribution quite similar to that of raw samples, from −24.54 to −22.32‰ (Figs. 8, 9). The open-system heated coal-bearing rocks show a narrower TC range, from 0.6 to 3.9%, with $\delta^{13}C_{TC}$ values ranging from −21.42 to −19.23‰, whereas the same rocks heated in the semi-closed system are characterised by TC values ranging from 18.9–24.5%, with a broader range of $\delta^{13}C_{TC}$ values from −26.14 to −22.05‰, the same as for raw samples (Figs. 8, 9).

Earlier laboratory experiments focused on the relationships between coal-CO_2 isotopic signatures (Warwick and Ruppert, 2016) and between the interactions of coal-CO_2-combustion products (Widory, 2006). Warwick and Ruppert (2016) postulated that the carbon isotopic signatures of CO_2 from coal combustion are similar to the signature of bulk coal, whereas Widory (2006) documented the fact that combustion gases are depleted in ^{13}C at a rate of approximately −1.3‰ compared to the source fuel. Moreover, both gaseous products, such as carbon oxides

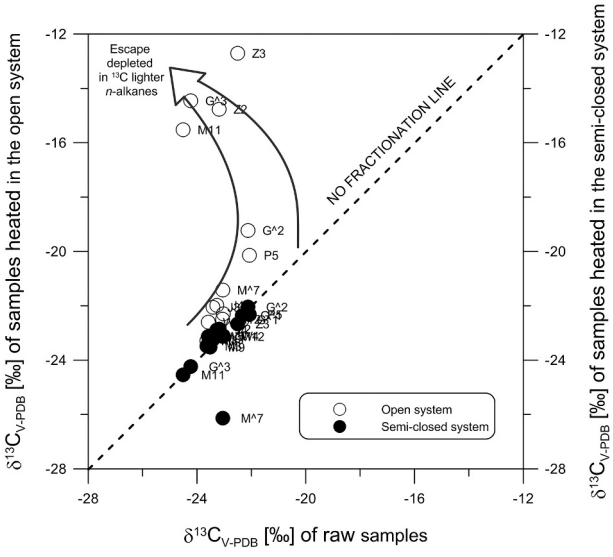

Fig. 8. The relation between carbon-isotope concentrations in raw samples and samples heated in the open- and semi-closed systems.

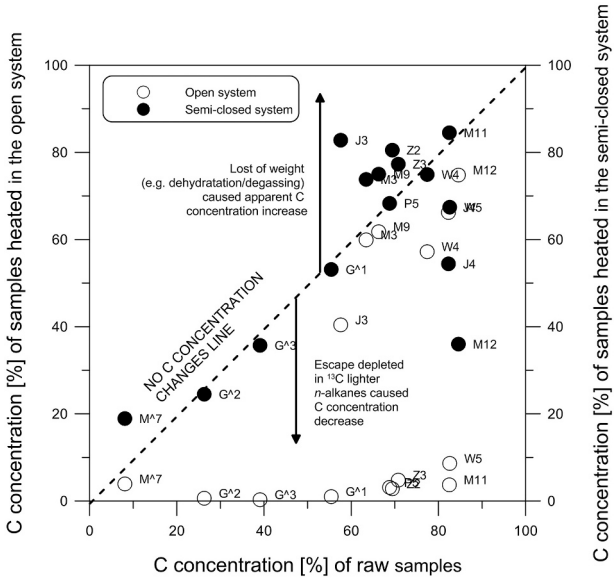

Fig. 9. The relation between carbon concentration in raw coal and coal heated in open- and semi-closed systems.

and solids (coke and soot), are formed if the system is nearly closed. In such systems, enrichment in ^{13}C in the solid-products-fuel-CO_2 sequence is observed (Widory, 2006). However, particles from coal combustion (unburned carbon phases) are characterised by $\Delta^{13}C_{gas\text{-}to\text{-}fuels}$ values close to 0 (Widory, 2006) or even slightly negative ($\delta^{13}C = -0.3 \pm 0.9$‰). Thus we expected similar variations in coal heated in the semi-closed system. Moreover, in the course of pyrolysis from 100 to 400 °C, the final carbon isotope composition may also have been modified; above ~400 °C, polyaromatisation is dominant and ^{13}C may be preferentially lost during the formation of C═C bonds, increasing the potential for further $\delta^{13}C$ residuum depletion (Bird and Ascough, 2012; Krull et al., 2003; Qian et al., 1992). Laboratory shale pyrolysis conducted by Conkright and Sackett (1992) resulted in

^{13}C-enrichment of the residuum due to (i) selective loss of ^{13}C-depleted aliphatic functional groups (e.g., lipids converted to thermogenic methane), (ii) selective loss of chemical functional groups and (iii) preferential dilacerating of relatively weak ^{12}C—^{12}C bonds and removal of cracking products depleted in ^{13}C (Schimmelmann et al., 2009).

The experimental heating of the coal and coal-bearing rocks in open and semi-closed systems confirmed differences in final isotopic signatures due to differences in heating conditions (Table 1; Figs. 8, 9). We expected that the post-heating residuum from the semi-closed system would exhibit the same- or similar carbon isotopic composition and TC contents as the raw coals and shales since a relatively low organic matter percentage would decay to gas. Schimmelmann et al. (2009) experiment involving heating on short one- week and long five-year time scales indicated negligible (0.3‰) fractionation of carbon isotopes. Similarly (assuming semi-closed natural system), $\delta^{13}C_{TC}$ values of coal samples from the Illinois Basin noted in Rahman et al. (2018) were only slightly enriched in ^{13}C near the dike front, whereas coal-bearing samples (shales) showed significant enrichment (1.2‰) in ^{13}C within 2 m of the intrusion.

In almost all our samples, carbon-isotope fractionation was either non-existent or negligible (Table 1; Fig. 8). Surprisingly, coal-bearing sample M^7 displayed significant isotopic depletion ca 3‰ (Fig. 8) with an increased C content after heating (Table 1; Fig. 9). It may be assumed that ^{13}C depletion was caused by kerogen aromatisation, whereas the apparent C content increase (see Fig. 9) was caused by weight loss due to the dehydration and/or degassing of clay minerals dominant in the sample. Rahman et al. (2018) described some TOC content increasing with depletion in ^{13}C c.a. 3–4 m from the dike caused

by the same processes. Finally, our observations based on the conducted experiments confirm that the kind of samples (coal or coal-bearing) and distance from possible temperature sources (e.g. dike, intrusion or palaeofire) play a crucial role in a proper interpretation of geological palaeo-history.

In contrast to the semi-closed system, we expected, in the open-system residuum, to find significant enrichment in ^{13}C as well as reduced C contents compared to the raw coal and coal-bearing rocks. Our hypothesis was tested and confirmed. The samples undergoing the most significant change (e.g., Z2, Z3, Gˆ3, M11 – see Fig. 8) belong to both groups and showed significant isotopic fractionation ca 9–10‰ with a substantial change in C contents (ca 90–99%; Fig. 9). C-isotope fractionation in the open system was probably caused by the escape of ^{13}C-depleted light *n*-alkanes, CH_4 degassing and preferential oxidising of ^{12}C to CO_2. In this case, our laboratory heating experiment is at odds with the observations of Rahman et al. (2018), where coal-bearing rocks revealed notable isotopic changes in comparison with coal.

Many have investigated coals and coal-bearing rocks that underwent a thermal change due to contact with an igneous intrusion (e.g., Mastalerz et al., 2009; Rahman et al., 2017, 2018; Schimmelmann et al., 2009; Yoksoulian et al., 2016) or hot fluids migrating through low-rank coal (Valentim et al., 2020). The noticeable thermal impact of a dike intrusion on a coal bed is typically limited to ~6–15 m. Values of $\delta^{13}C$ show ambiguous-, stable-, or decreasing trends compared to unaltered coals (Rahman et al., 2017; Yoksoulian et al., 2016). Rahman et al. (2017) indicated no significant or negligible changes in coal carbon-isotope composition caused by an intrusion, whereas Schimmelmann et al. (2009) and Mastalerz et al. (2009) found sinusoidal fluctuations with a notable amplitude of ~2‰. Less(c.a. 1.2‰) but similar carbon isotopes fluctuation was reported in Rahman et al. (2018) for coal-bearing (shale) rocks. Some changes were probably associated with the loss of volatile pyrolysates, with the result that only small amounts of extractable bitumen remained in the coal. In contrast, some pyrolysate components precipitated at a distance of 4–5 m from the contact at moderate temperature and produced the highest concentration of bitumen in the analysed coal (Schimmelmann et al., 2009). Thus, the sampling location is crucial to the correct interpretation of possible maturation processes.

Based on our laboratory investigations and recent findings on heating processes preserved in coals and coal-bearing rocks, we attempt to identify locations potentially affected by heating within a coal deposit (Fig. 10). Referencing our samples, the most probable intra-deposit heating sites are:

1) At a depth of 765–782 m - the Gˆ1 (501 seam) and G2 (502 seam) samples characterised by the lowest %C (<60% TC) and enrichment in ^{13}C relative to average (−23.26 ± 0.67‰) and the highest R_r (>0.83). These locations may represent the innermost front of an underground fire in semi-open conditions.
2) At a depth of 898 m - the Gˆ3 sample characterised by the lowest %C (<60% TC) and depletion in ^{13}C relative to average (-23.26 ± 0.67‰) and the highest R_r (>0.83). In our opinion, Gˆ3 may represent a location farther from the heating centre in semi-open conditions where some pyrolysate components precipitated, and the highest depletion in ^{13}C bitumen in coal was produced (compare to Schimmelmann et al., 2009)
3) The J3 sample (503 seam) characterised by the lowest %C (slightly below 60% TC) and highest R_r (> 0.83) but with no observable changes in $\delta^{13}C_{TC}$. This sample may represent a semi-closed system similar to our semi-closed experiment.

4. Conclusions

The laboratory experiment of heating in both open and semi-closed systems was conducted to identify alterations occurring in the stable carbon isotopic signature-, organic petrography and geochemistry of organic matter. The results potentially enable the identification of the effects of underground heating caused by an intra-deposit fire on organic matter-rich rocks. They may also aid the assessment of heating conditions, i.e., whether heating occurred in an open system with oxygen access and volatile-product escape or in a closed/semi-closed system with restricted oxygen access and retention of volatiles (pyrolysis).

The crucial influence of temperature and oxygen access on organic compounds' behaviour and $\delta^{13}C$ values was confirmed. Coals subjected to underground heating are characterised by: (i) nearly the same $\delta^{13}C$ value as unaltered coal, with possible increases or decreases in C content in the closed or semi-closed underground system; (ii) enrichment in ^{13}C (up to 10‰) compared to unaltered coal, with very low C concentrations in the case of underground heating with essentially unrestricted oxygen access.

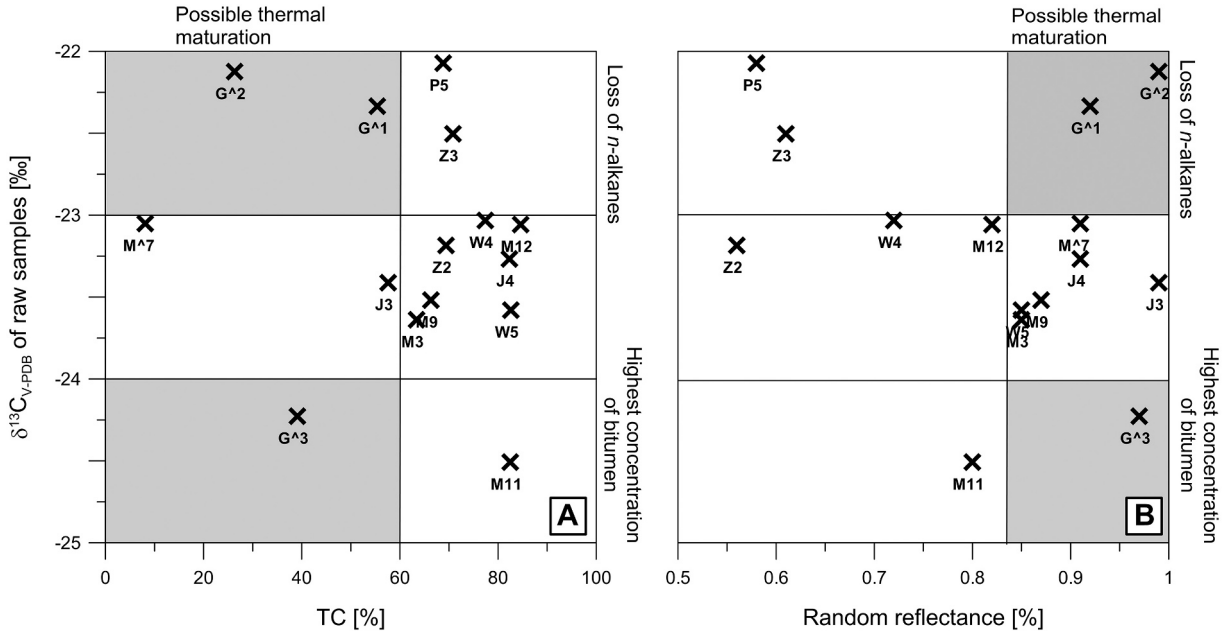

Fig. 10. The relation between total carbon concentration (a) and random reflectance (b) in raw samples.

Significant differences in $\delta^{13}C$ values, ranging from 0.18–9.79‰, occur with open- system heating of coal; released ^{13}C-depleted gases enrich residue coke in ^{13}C compared to raw coal. In organic geochemistry, the significant indicators of such conditions are depletion in extractable compounds to the level < 0.02 wt% and the absence or near absence of low-molecular-weight organic compounds such as biphenyl, naphthalene derivatives, and *n*-alkanes showing ~10–20% relative depletion in the n-C_{11}-n-C_{18} range. With open-system heating, removing these ^{12}C-rich compounds causes significant enrichment of the post-heating residuum in ^{13}C, and a wide range of $\delta^{13}C_{TC}$ values are measured for the residuum. The distribution of *n*-alkanes does not show the Gaussian outline typical of pyrolytic conditions but a bimodal outline characteristic of kerogen III. Probably, the extractable compounds derive from residual pore bitumen and retain some features of kerogen III. If PAHs are present, a relatively high proportion of combustion-formed PAHs is a further indicator of such heating.

With a semi-closed system, there were no changes in isotopic composition. No components are carried away. Scales of changes in petrographic- and geochemical form are as known for natural coals. Organic matter shows an increase in extract yields due to bitumen release from closed pores and, possibly, partial pyrolysis of organic matter. The outline of *n*-alkanes is Gaussian or semi-Gaussian, with some depletion in lighter compounds. No *n*-alken-1-es, typical pyrolytic compounds, were produced possibly due to low temperatures. Variable and inconsistent values of various alkyl aromatic hydrocarbon ratios, and their discrepancies relative to increased R_r values, constitute another indicator of semi-closed heating. Only slight depletion in lighter compounds is reflected in negligible (0.3‰) carbon-isotope fractionation.

The experiments enabled us to attempt a reconstruction of conditions in coal seams with reduced thicknesses. Rocks suspected of having undergone intra-deposit heating showed geochemical- and isotopic features indicating semi-closed- rather than open-system heating; Rr increases, depletion of C and volatiles are depleted, *n*-alkane outlines change, and Pr/n-C_{17} and Ph/n-C_{18} values shift. Rocks heated earlier in an intra-deposit fire do not respond strongly when re-heated. When very light compounds remained, a closed-system could be assumed when, in some such cases, whereas, in others, light-compound depletion was indicative of a semi-closed system.

The impact of palaeofires was not seen in the maceral and mineral matter properties of coal, but the heating experiments caused devolatilisation pores, rounded edges, cracks, pale rims, and higher reflectance and paler colour that was what was expected.

Conclusions on the thermal history of coal, even when based on experiment, isotope composition, petrography and geochemistry, are challenging; the many rock and environmental variables are difficult to untangle. However, the influence of intra-deposit palaeoheating of coal seams was recognised by the organic geochemistry and $\delta^{13}C$ data.

Declaration of Competing Interest

The authors declare no conflict of interest.

Acknowledgements

The project was funded from grant 2016/21/B/ST10/02293 from the National Science Centre, Poland. Dr Pádhraig Kennan (University College Dublin, Ireland) is thanked for language correction.

References

Arora, A., Dutta, S., Gogoi, B., Banerjee, S., 2017. The effects of igneous dike intrusion on organic geochemistry of black shale and its implications: late Jurassic Jhuran Formation, India. Int. J. Coal Geol. 178, 84–99.

Benner, R., Fogel, M.L., Sprague, E.K., Hodson, R.E., 1987. Depletion of C in lignin and its implications for stable carbon isotope studies. Nature 329, 708–710.

Bird, M.I., Ascough, P.L., 2012. Isotopes in pyrogenic carbon: a review. Org. Geochem. 42, 1529–1539.

Brasseur, A., Antenucci, D., Bouquegneau, J.M., Coëme, A., Dauby, P., Létolle, R., Mostade, M., Pirlot, P., Pirard, J.P., 2002. Carbon stable isotope analysis as a tool for tracing temperature during the El Tremedal underground coal gasification at great depth. Fuel 81, 109–117.

Bray, E.E., Evans, E.D., 1963. Distribution of *n*-paraffins as a clue to recognition of source beds. Geochim. Cosmochim. Acta 22, 2–15.

ChemSpider, 2021. http://www.chemspider.com/Chemical-Structure.12863.html.

ChemSrc, 2021. https://www.chemsrc.com/.

Ciesielczuk, J., Fabiańska, M.J., Misz-Kennan, M., Jura, Kruszewski, Ł., 2017. Thermally-affected Carboniferous Sediments Overlying Thinned Coal Seams in Jastrzębie Mine (Poland). https://goldschmidtabstracts.info/2017/697.pdf.

Ciesielczuk, J., Nawrocki, J., Jura, D., Fabiańska, M.J., Misz-Kennan, M., Filipiak, P., 2020. Probable Time and Conditions of a Coal-Seam Paleofire in the Upper Silesian Coal Basin, Poland. goldschmidtabstracts.info/2020/445.pdf. doi.org/10.46427/gold2020.445.

Conkright, M.E., Sackett, W.M., 1992. Stable carbon isotope changes during the maturation of organic matter. In: Whelan, J., Farringtou, J.W. (Eds.), Organic Matter. Columbia Press, pp. 403–416.

Coplen, T.B., Brand, W.A., Gehre, M., Gröning, M., Meijer, H.A.J., Toman, B., Verkouteren, R.M., 2006. New guidelines for $\delta^{13}C$ measurements. Anal. Chem. 78 (7), 2439–2441.

Dai, S., Graham, I.T., Ward, C.R., 2016. A review of anomalous rare earth elements and yttrium in coal. Int. J. Coal Geol. 159, 82–95.

Didyk, B.M., Simoneit, B.R.T., Brassell, S.C., Eglington, G., 1978. Organic geochemical indicators of palaeoenvironmental conditions of sedimentation. Nature 272, 216–222.

Engle, M.A., Radke, L.F., Heffern, E.L., O'Keefe, J.M.K., Hower, J.C., Smeltzer, C.D., Hower, J.M., Olea, R.A., Eatwell, R.J., Blake, D.R., Emsbo-Mattingly, S.D., Stout, S. A., Queen, G., Aggen, K.L., Kolker, A., Prakash, A., Henke, K.R., Stracher, G.B., Schroeder, P.A., Román-Colón, Y., ter Schure, A., 2012. Gas emissions, minerals, and tars associated with three coal fires, Powder River Basin. USA. Sci. Total Environ. 420, 146–159.

Fabiańska, M.J., Ćmiel, S., Misz-Kennan, M., 2013. Biomarkers and aromatic hydrocarbons in bituminous coals of Upper Silesian Coal Basin: example from 405 coal seam of the Zaleskie Beds (Poland). Int. J. Coal Geol. 107, 96–111.

Finkelman, R.B., Dai, S., French, D., 2019. The importance of minerals in coal as the hosts of chemical elements. Int. J. Coal Geol. 212, 103251.

Gabzdyl, W., Probierz, K., 1987. The occurrence of anthracites in the area characterised by low rank coals in the Upper Silesian Coal Basin of Poland. Int. J. Coal Geol. 7, 209–225.

Gabzdyl, W., Hanak, B., Probierz, K., Kubik, A., 1997. Rank, petrographic composition and chemical-technological properties of coal seams from the Upper Silesian Coal Basin. Prace Państwowego Instytutu Geologicznego Warsaw 67, 319–326.

Goodarzi, F., Murchison, D.G., 1978. Influence of heating-rate on the anisotropy of carbonised vitrinites. Fuel 57 (5), 273–284.

Goossens, H., de Leeuw, J.W., Schenck, P.A., Brassell, S.C., 1984. Tocopherols as likely precursors of pristane in ancient sediments and crude oils. Nature 312, 440–442.

Guo, X., Tang, Y., Eble, C.F., Wang, Y., Li, P., 2020. Study on petrographic characteristics of devolatilisation char/coke related to coal rank and coal maceral. Int. J. Coal Geol. 227, 103504.

Heffern, E.L., Coates, D.A., 2004. Geologic history of natural coal-bed fires, Powder River basin. USA. Int. J. Coal Geol. 59 (1–2), 25–47.

International Committee for Coal and Organic Petrology, 1998. New vitrinite classification (ICCP system 1994). Fuel 77, 349–358.

International Committee for Coal and Organic Petrology, 2001. New inertinite classification (ICCP system 1994). Fuel 80, 459–471.

ISO 7404-2, 2009. Methods for the Petrographic Analysis of Coals – Part 2: Methods of Preparing Coal Samples. International Organization for Standardization, Switzerland, 12 pp.

ISO 7404-3, 2009. Methods for the Petrographic Analysis of Coals – Part 3: Method of Determining Maceral Group Composition. International Organization for Standardization, Geneva, Switzerland, 7 pp.

ISO 7404-5, 2009. Methods for the Petrographic Analysis of Coals - Part 5: Method of Determining Microscopically the Reflectance of Vitrinite. International Organization for Standardization, Switzerland, 11 pp.

Jura, D., 2001. Morphotectonics and evolution of discordances of different age present in the top surface of the Carboniferous of the Upper Silesian Coal Basin. Publishing House of the University of Silesia in Katowice, p. 176 [in polish with English abstract]. http://www.sbc.org.pl/Content/61402/morfotektonika_i_ewolucja.pdf.

Jurczak-Drabek, A., 1996. Petrographical Atlas of Coal Deposits, Upper Silesian Coal Basin 1:300000. Polish Geological Institute, Warsaw, 31 pp.

Jureczka, J., Kotas, A., 1995. Coal deposits. Upper Silesian Coal Basin. In: Zdanowski, A., Żakowa, H. (Eds.), The Carboniferous System in Poland. Publication of Polish Geological Institute, Warsaw, pp. 164–173.

Jureczka, J., Dopita, M., Gałka, M., Krieger, W., Kwarciński, J., Martinec, P., 2005. Geological Atlas of Coal Deposits of the Polish and Czech Parts of the Upper Silesian Coal Basin. Polish Geological Institute, Warsaw, 31 pp.

Klika, Z., Kraussová, J., 1993. Properties of altered coals associated with Carboniferous red beds in the Upper Silesian Coal Basin and their tentative classification. Int. J. Coal Geol. 22 (3–4), 217–235.

Klika, Z., Kozubek, T., Martinec, P., Kliková, Ch., Dostál, Z., 2004. Mathematical modelling of bituminous coal seams burning contemporaneously with the formation of a variegated beds body. Int. J. Coal Geol. 59, 137–151.

Kotarba, M.J., Clayton, J.L., 2003. A stable carbon isotope and biological marker study of polish bituminous coals and carbonaceous shales. Int. J. Coal Geol. 55 (2–4), 73–94.
Křibek, B., Sýkorová, I., Veselovský, F., Laufek, F., Malec, J., Knésl, I., Majer, V., 2017. Trace element geochemistry of self-burning and weathering of a mineralized coal waste dump: the Novátor mine, Czech Republic. Int. J. Coal Geol. 173, 158–175.
Krull, E.S., Skjemstad, J.O., Graetz, D., Grice, K., Dunning, W., Cook, G., Parr, J.F., 2003. ^{13}C-depleted charcoal from C4 grasses and the role of occluded carbon in phytoliths. Org. Geochem. 34, 1337–1352.
Kus, J., 2017a. Impact of underground coal fire on coal petrographic properties of high volatile bituminous coals: a case study from coal fire zone no. 3.2 in the Wuda Coalfield, Inner Mongolia Autonomous Region, North China. Int. J. Coal Geol. 171, 185–211.
Kus, J., 2017b. Oxidatively and thermally altered high-volatile bituminous coals in high temperature coal fire zone no. 8 of the Wuda Coalfield (North China). Int. J. Coal Geol. 176–177, 8–35.
Kus, J., Misz-Kennan, M., ICCP, 2017. Coal weathering and laboratory (artificial) coal oxidation. Int. J. Coal Geol. 171, 12–36.
Kwiecińska, B., Petersen, H.I., 2004. Graphite, semi-graphite, natural coke, and natural char classification-ICCP system. Int. J. Coal Geol. 57, 99–116.
Leythauser, D., Schwartzkopf, Th., 1985. The pristane/*n*-heptadecane ratio as an indicator for recognition of hydrocarbon migration effects. Org. Geochem. 10, 191–197.
Liu, D., Yu, Z., Lin, J., 2018. Application of combustion module coupled with cavity ring-down spectroscopy for simultaneous measurement of SOC and δ^{13}C-SOC. J. Spectrosc. 2018, 5. Article ID 6893454.
Martinec, P., Jirásek, J., Kožušniková, A., Sivek, M. (Eds.), 2005. Atlas of Coal - the Czech Part of the Upper Silesian Basin. Anagram, Ostrava, 64 pp.
Mastalerz, M., Drobniak, A., Schimmelmann, A., 2009. Changes in optical properties, chemistry, and micropore and mesopore characteristics of bituminous coal at the contact with dikes in the Illinois Basin. Int. J. Coal Geol. 77 (3–4), 310–319.
Misz-Kennan, M., 2010. Thermal alterations of organic matter in coal wastes from Upper Silesia, Poland. Mineralogia 41 (3–4), 105–236.
Misz-Kennan, M., Fabiańska, M.J., 2010. Thermal transformation of organic matter in coal waste from Rymer Cones (Upper Silesian Coal Basin, Poland). Int. J. Coal Geol. 81, 343–358.
Misz-Kennan, M., Fabiańska, M.J., 2011. Application of organic petrology and geochemistry to coal waste studies. Int. J. Coal Geol. 88, 1–23.
Misz-Kennan, M., Kus, J., Flores, D., Avila, C., Büçkün, Z., Choudhury, N., Christanis, K., Joubert, J.P., Kalaitzidis, S., Karayigit, A.I., Malecha, M., Marques, M., Martizzi, P., O'Keefe, J.M.K., Pickel, W., Predeanu, G., Pusz, S., Ribeiro, J., Rodrigues, S., Singh, A.K., Suárez-Ruiz, I., Sýkorová, I., Wagner, N.J., Životić, D., ICCP, 2020. Development of a petrographic classification system for organic particles affected by self-heating in coal waste. (An ICCP Classification System, Self-heating Working Group–Commission III). Int. J. Coal Geol. 220, 103411.
MSD, 2012. The Wiley Registry of Mass Spectral Data, 10th ed. Wiley, New York.
Murchison, D., 2006. The influence of heating rates on organic matter in laboratory and natural environments. Int. J. Coal Geol. 67 (3), 145–157.
Muszyński, M., Skowroński, A., Lipiarski, I., 2006. Red beds of the collapse-type breccia from the "Marcel" Coal Mine (Upper Silesian Coal Basin, Poland). Geologia 32 (3), 345–367 (in Polish with English abstract).
Parzentny, H.R., 2020. Spatial macroscale variability of the role of mineral matter in concentrating some trace elements in bituminous coal in a Coal Basin – a case study from the Upper Silesian Coal Basin in Poland. Minerals 10 (5), 422.
Patra, S., Sitindra, S.D., Arka, R., Dutta, S., Ghosh, S., Varma, A., Shome, D., Kalpana, M., 2018. Effects of thermal maturity on biomarker distributions in Gondwana coals from the Satpura and Damodar Valley Basins, India. Int. J. Coal Geol. 196, 63–81.
Peters, K.E., Walters, C.C., Moldowan, J.M., 2005. The Biomarker Guide. Biomarkers and isotopes in petroleum exploration and earth history. In: Petroleum Geochemistry, , 2nd ed2. Cambridge University Press, pp. 141–203.
Philp, R.P., 1985. Fossil Fuel Biomarkers. Application and Spectra. Elsevier, Amsterdam, 294 pp.
Pickel, W., Kus, J., Flores, D., Kalaitzidis, S., Christanis, K., Cardott, B.J., Misz-Kennan, M., Rodrigues, S., Hentschel, A., Hamor-Vido, M., Crosdale, P., Wagner, N., ICCP, 2017. Classification of liptinite – ICCP system 1994. Int. J. Coal Geol. 169, 40–61.
Qian, Y., Engel, M.H., Macko, S.A., 1992. Stable isotope fractionation of biomonomers during protokerogen formation. Chem. Geol. 101, 201–210.
Radke, M., 1987. Organic geochemistry of aromatic hydrocarbons. In: Brooks, J., Welte, D.H. (Eds.), Advances in Petroleum Geochemistry 2. New York, Academic Press, pp. 141–207.
Radke, M., Welte, D.H., 1983. The methylphenanthrene index (MPI): a maturity parameter based on aromatic hydrocarbons. In: Bjorùy, M. (Ed.), Advances in Organic Geochemistry, pp. 504–512. Chichester.
Rahman, M.W., Rimmer, S.M., Rowe, H.D., Huggett, W.W., 2017. Carbon isotope analysis of whole-coal and vitrinite from intruded coals from the Illinois Basin: no isotopic evidence for thermogenic methane generation. Chem. Geol. 453, 1–11.
Rahman, M.W., Rimmer, S.M., Rowe, H.D., 2018. The impact of rapid heating by intrusion on the geochemistry and petrography of coals and organic-rich shales in the Illinois Basin. Int. J. Coal Geol. 187, 45–53.
Richardson, A.R., Eble, C.F., Hower, J.C., O'Keefe, J.M.K., 2012. A critical re-examination of the petrology of the no. 5 Block coal in eastern Kentucky with special attention to the origin of inertinite macerals in the splint lithotypes. Int. J. Coal Geol. 98, 41–49.
Rimmer, S.M., Rowe, H.D., Taulbee, D.N., Hower, J.C., 2006. Influence of maceral content on δ^{13}C and δ^{15}N in a Middle Pennsylvanian coal. Chem. Geol. 225 (1–2), 77–90.
Sanders, M.M., Rimmer, S.M., 2020. Revisiting the thermally metamorphosed coals of the Transantarctic Mountains, Antarctica. Int. J. Coal Geol. 228, 103550.
Schimmelmann, A., Mastalerz, M., Gao, L., Sauer, P.E., Topalov, K., 2009. Dike intrusions into bituminous coal, Illinois Basin: H, C, N, O isotopic responses to rapid and brief heating. Geochim. Cosmochim. Ac. 73, 6264–6281.
Scott, A.C., 2000. The Pre-Quaternary history of fire. Palaeogeogr. Palaeoclimatol. Palaeoecol. 164, 281–329.
Scott, A.C., 2018. Burning planet. In: The Story of Fire Through Time. Oxford University Press, p. 243.
Scott, A.C., Glasspool, I.J., 2007. Observations and experiments on the origin and formation of inertinite group macerals. Int. J. Coal Geol. 70, 53–66.
Scott, A.C., Jones, T.P., 1991. Fossil charcoal: a plant-fossil record of preserved fire. Geol. Today 7 (6), 214–216.
Seifert, W.K., Moldowan, J.M., 1986. Use of biological markers in petroleum exploration. In: Johns, R.B. (Ed.), Methods in Geochemistry and Geophysics, 24. Elsevier, Amsterdam, pp. 261–290.
Seredin, V.V., Dai, S., 2012. Coal deposits as potential alternative sources for lanthanides and yttrium. Int. J. Coal Geol. 94, 67–93.
Shanmungam, G., 1985. Significance of coniferous rain forests and related organic matter in generating commercial quantities of oil, Gippsland Basin, Australia. AAPG Bull. 69, 1241–1254.
Simoneit, B.R.T., 1993. Hydrothermal Alteration of Organic Matter in Marine and Terrestrial Systems. In: Engel, M.H., Macko, S.A. (Eds.), Organic Geochemistry, Principles and Applications. Plenum Press, New York, pp. 397–418.
Skrzypek, G., 2013. Normalisation procedures and reference material selection in stable HCNOS isotope analyses: an overview. Anal. Bioanal. Chem. 405, 2815–2823.
Sokol, E.V., Maksimova, N.V., Nigmatulina, E.N., Sharygin, V.V., Kalugin, V.M., 2005. Combustion Metamorphism. Publishing House of the SB RAS, Novosibirsk, Russia, p. 312 [In Russian, with some English Abstracts].
Stracher, G.B., Prakash, A., Sokol, E.V., 2011. Coal and Peat Fires: A Global Perspective, 1st ed. Elsevier, Amsterdam, The Netherlands. 357 pp.
Suárez-Ruiz, I., Crelling, J., 2008. Applied Coal Petrology. The Role of Petrology in Coal Utilization. Elsevier, Amsterdam, 388 pp.
Suárez-Ruiz, I., Diez, M.A., Rubeira, F., 2019. New trends in coal conversion. In: Combustion, Gassification, and Coking. Woodhead Publishing Series in, Energy, Elsevier, United Kingdom, 511 pp.
Taylor, G.H., Teichmüller, M., Davis, A., Diessel, C.F.K., Littke, R., Robert, R., 1998. Organic Petrology. A New Handbook Incorporating some Revised Parts of Stach's Textbook of Coal Petrology. Gebrüder Borntraeger, Berlin, 704 pp.
Tissot, B.P., Welte, D.H., 1984. Petroleum Formation and Occurrence. Springer Verlag, Berlin, 677 pp.
Valentim, B., Couto, H., French, D., Golding, S.D., Guimarães, F., Guedes, A., O'Keefe, J. M.K., Raymond, A.L., Santos, C., Valian, A., Ward, C.R., Hower, J.C., 2020. Could hot fluids be the cause of natural pyrolysis at the ragged edge of Herrin coal, Millport 7 ½' quadrangle, Hopkins County, Kentucky? Int. J. Coal Geol. 231, 103603.
Ward, C.R., 2002. Analysis and significance of mineral matter in coal seams. Int. J. Coal Geol. 50, 135–168.
Ward, C.R., 2016. Analysis, origin and significance of mineral matter in coal: an updated review. Int. J. Coal Geol. 165, 1–27.
Warwick, P.D., Ruppert, L.F., 2016. Carbon and oxygen isotopic composition of coal and carbon dioxide derived from laboratory coal combustion: a preliminary study. Int. J. Coal Geol. 166, 128–135.
Widory, D., 2006. Combustibles, fuels and their combustion products: a view through carbon isotopes. Combust. Theory Model. 10, 831–841.
Yoksoulian, L.E., Rimmer, S.M., Rowe, H.D., 2016. Anatomy of an intruded coal, II: effect of contact metamorphism on organic δ13C and implications for the release of thermogenic methane, Springfield (no. 5) Coal, Illinois Basin. Int. J. Coal Geol. 158, 129–136.
Zdanowski, A., Żakowa, H. (Eds.), 1995. The Carboniferous System in Poland. Publication of Polish Geological Institute, Warsaw, 215 pp.

Further-reading

Kotarba, M.J., Clayton, J.L., Rice, D.D., Wagner, M., 2002. Assessment of hydrocarbon source rock potential of polish bituminous coals and carbonaceous shales. Chem. Geol. 184, 11–35.